Title: **Statistical properties of threshold and notch derived estimations of the critical distance according to the line method of the theory of critical distances**

Authors: **M. Benedetti, C. Santus**

Statistical properties of threshold and notch derived estimations of the critical distance according to the Line Method of the Theory of Critical Distances

M. Benedetti[a], C. Santus[b*]

[a] Department of Industrial Engineering – DII, University of Trento, Italy

[b] Department of Civil and Industrial Engineering – DICI, University of Pisa, Italy

* Corresponding author

Ciro Santus

ciro.santus@ing.unipi.it

Abstract

The theory of critical distances is based on the definition of a material-dependent length L. Here, we investigate the statistical properties of L deduced from the crack threshold or a suitable notched specimen geometry. Monte Carlo simulations are done for best-fitting analytical functions to express mean, standard deviation and skewness of L. Standard-deviation-to-mean ratio is the lowest for the threshold-derived L estimation and decreases with notch sharpness. The minimum notch severity to achieve the desired accuracy in L estimation is identified. The impact of these statistical properties on the prediction of independent notched and cracked configurations is evaluated.

Keywords

Critical distance; notch fatigue; crack growth threshold; statistics; Monte Carlo simulations.

Nomenclature

CV	coefficient of variation (standard deviation to mean ratio)
D	specimen outer diameter
K_f	fatigue stress concentration factor
K_N	notch-stress intensity factor (N-SIF)
$K_{N,UU}$	N-SIF for unitary nominal stress and unitary half-diameter D
l	dimensionless notch-derived critical distance (Eq. (6a))
l_0	dimensionless notch-derived critical distance for an infinitely sharp notch (Eq. (6d))
$\overline{l}$	dimensionless notch-derived critical distance obtained from mean values of plain and notch fatigue limit

l_{lim} notch-derived limit critical distance corresponding to a given value of NCV ν

l_{min} minimum limit for the range of accurate notch-derived critical distance estimation

l_{max} maximum limit for the range of accurate notch-derived critical distance estimation

l_{th} dimensionless threshold-derived critical distance (Eq. (6a))

$\overline{l}_{th}$ dimensionless threshold-derived critical distance obtained from mean values of plain fatigue limit and crack threshold

L notch-derived critical distance

L_{th} threshold-derived critical distance

LM line method

MC Monte Carlo

NCV normalized coefficient of variation

PDF probability density function

r CV of plain fatigue limit range

r_N CV of notch fatigue limit range

r_{th} CV of threshold stress intensity factor range

R notch radius

R stress ratio

s William's power law singularity exponent

S, S_N, S_{th} standard deviation of plain and notch fatigue limit as well as crack growth threshold, respectively

sk skewness of dimensionless notch-derived critical distance

sk_{th} skewness of dimensionless threshold-derived critical distance

SND skew-normal distribution

TCD theory of critical distances

α shape parameter of the skew-normal distribution (Eq. (10a))

$\overline{\alpha}$ notch opening angle

β location parameter of the skew-normal distribution (Eq. (10a))

δ standard deviation of dimensionless notch-derived critical distance

δ_{th} standard deviation of dimensionless threshold-derived critical distance

ΔK_{th} threshold stress intensity factor range. In this work, it is assumed to be normally distributed with mean $\Delta\overline{K}_{th}$ and standard deviation S_{th}

$\Delta\sigma_{fl}$ plain specimen fatigue limit range. In this work, it is assumed to be normally distributed with mean $\Delta\overline{\sigma}_{fl}$ and standard deviation S

$\Delta\sigma_{N,fl}$ notched specimen fatigue limit range (net nominal stress). In this work, it is assumed to be normally distributed with mean $\Delta\bar{\sigma}_{N,fl}$ and standard deviation S_N

ε fluctuation index of a certain statistical property p (Eq. (9))

φ line slope of the LM inversion function

γ scale parameter of the skew-normal distribution (Eq. (10a))

κ r_N to r ratio

κ_{th} r_{th} to r ratio

λ_{min} minimum value of the inversion function range

λ_{max} maximum value of the inversion function range

μ mean of dimensionless notch-derived critical distance

μ_{th} mean of dimensionless threshold-derived critical distance

ν CV of the notch-derived critical length normalized to the equivalent CV of the input data Σ

ν_0 NCV of the notch-derived critical length for an infinitely sharp notch

ν_{th} CV of the threshold-derived critical length normalized to the equivalent CV of the input data Σ_{th}

ρ dimensionless notch radius (Eq. (6a))

ρ_{lim} dimensionless notch radius corresponding to a given value of NCV (Eq. (13c))

Σ equivalent CV of input data for notch-derived critical length estimation (Eq. (11a))

Σ_{th} equivalent CV of input data for threshold-derived critical length estimation (Eq. (11a))

Best-fit coefficients

$a_1,...,a_4$ skewness inversion function (Eq. (10e))

b_1,b_2 limit critical distance (Eq. (12b))

c_1,c_2,c_3 model function coefficients for l_{max} (Eq. (7d))

d normalized standard deviation on the estimation of crack threshold based on notch-derived critical length estimations (Eq. (15b))

d_{th} normalized standard deviation on the estimation of crack threshold limit based on threshold-derived critical length estimations (Eq. (15a))

$f_1,...,f_6$ normalized standard deviation on the estimation of notch fatigue limit based on notch-derived critical length estimations (Eq. (14b)).

$f_{th,1},...,f_{th,6}$ normalized standard deviation on the estimation of notch fatigue limit based on threshold-derived critical length estimations (Eq. (14a)).

m_1,m_2 Mean of notch-derived critical length estimation (Eq. (13d))

$m_{th,1}$,$m_{th,2}$ Mean of threshold-derived critical length estimation (Eq. (12b))

n_1,...,n_4 NCV of notch-derived critical length estimation (Eq. (13d))

p_1,...,p_4 model function coefficients for l_{min} (Eq. (7b))

q_1,...,q_4 model function coefficients for λ_{min} (Eq. (7c))

s_1,s_2 Skewness of notch-derived critical distance estimation (Eq. (13f))

$s_{th,1}$,$s_{th,2}$ Skewness of threshold-derived critical distance estimation (Eq. (12c))

1. Introduction

The theory of critical distances (TCD) is a powerful tool for estimating the strength of notched components, just on the basis of standard material tests. There are different formalizations of the TCD, and the more common are the Point Method and the Line Method [1]. All the TCD techniques share the same length, i.e. the critical distance, which is a material property also depending on the fatigue stress ratio R[1]. Although in principle the TCD is defined for notches loaded under mode I, several extensions of this methodology have been applied. The TCD was combined with a multiaxial fatigue criterion, according to a critical plane approach by Susmel and Taylor [2]. Liao et al. [3] recently proposed the orientation of the critical distance length along the critical plane, instead of the notch bisector, and similarly was proposed by Santus [4] for the fretting fatigue application. In this way, more accurate results were obtained suggesting a better matching between the critical distance length and the highest stress path orientation.

The critical distance turns out to be coincident with the El Haddad length a_0, which is fictitiously added to the actual crack length for extending the long crack fracture mechanics to the small cracks. Moreover, the TCD length is also defined on the well-known Kitagawa-Takahashi diagram, as the intersection between the fatigue strength of the long crack and the fatigue limit of the unnotched (plain) specimen. This length is indeed obtained from the threshold Stress Intensity Factor (SIF) range ΔK_{th} and the full range fatigue limit of the plain specimen $\Delta\sigma_{fl}$, both experimentally obtained at the same stress ratio R:

$$L_{th} = \frac{1}{\pi}\left(\frac{\Delta K_{th}}{\Delta\sigma_{fl}}\right)^2 \tag{1}$$

The subscript “th” is usually not applied to the TCD length, however, in this study it refers to the determination of L by means of the threshold SIF range. On the contrary, the assessment of the critical distance with a sharp notch geometry is an alternative approach, deeply investigated by the authors in this paper and previous research. According to the basic definition of the critical distance, Eq. (1),

[1] In this paper the stress ratio is referred to as R, while the symbol R is used for the radius of the V-notched specimens.

in order to have a proper assessment of L_{th}, the threshold SIF range ΔK_{th} is required with enough accuracy. However, despite the standardized procedure provided by the ASTM E647 [5], this test is quite challenging, time consuming, and requires specific experience. Different effects can play a role when this testing is performed, such as the precracking strategy, as investigated by Forth et al. [6]. A slightly lower threshold is in fact obtained by applying the compression precracking constant amplitude method, with respect to the common load-reduction method, as shown by Jordon et al. [7] and Newman and Yamada [8]. The main issues are related to the plasticity-induced crack closure, as reviewed by Zerbst et al. [9, 10], which in principle can be considered and then modeled, as proposed by Noroozi et al. [11]. However, an intrinsic uncertainty of the effective SIF cycle experienced at the crack tip is unavoidable. Moreover, the environmental conditions are also well known to be quite effective, both for the threshold, and the crack growth rate.

For these reasons, the threshold ΔK_{th} may be not uniquely defined, thus its determination just for obtaining the critical distance, is not usual. On the contrary, this length is more easily obtained by combining the strength of two initially uncracked specimens and imposing a TCD criterion. Furthermore, the fracture mechanics properties can be then obtained without performing the specific tests. Susmel and Taylor in this way obtained ΔK_{th} values, as well as K_{Ic}, for several metal alloys and other materials [12]. They just inverted Eq. (1) after comparing the test results of standard specimens, according to the Point Method. The plain specimen and a notched specimen were considered for the fatigue properties, whilst they combined two notches with different sharpness to derive the fracture toughness. The use of a sharply-notched specimen, instead of the threshold SIF range for evaluating the fatigue critical distance L was clearly suggested by Taylor [13]. This approach can be found in several papers by different researchers, in particular dedicated to the brittle fracture (or “static”) properties. Thus, the comparison between two specimens with a significant difference in terms of notch sharpness, i.e. a blunt vs. a sharp notch, is actually the common practice [14, 15, 16, 17, 18, 19, 20]. Cicero et al. [21] recently proposed a comparison with more than just two notched specimens, dedicated to the brittle fracture properties determination, showing how accurate and robust is this method, based on the Point Method.

Santus et al. [22] emphasized the determination of the fatigue critical distance by combining a sharp notched specimen and the plain specimen. A dedicated V-notched specimen was proposed, with optimized notch depth, and proper values of notch angle and root radius were considered, also taking into account the manufacturing viability. Moreover, a complete numerical procedure was provided to calculate the critical distance value after the availability of the experimental fatigue stress concentration factor K_f. This inverse search procedure was both based on the Line and the Point Methods, and for the Line Method it turned out to be much easier and effective since a linear

relationship holds. Santus et al. [23] then provided a direct validation of this procedure, showing a more accurate prediction of the Line Method length L in terms of comparison with threshold-based length L_{th}. The critical distance has been extended to the medium-cycle fatigue regime, by assuming L as dependent on the number of cycles to failure. A power law relationship for the $L(N_f)$ function was proposed by Susmel and Taylor [14], followed by several other authors such as Negru et al. [24] and Wen et al. [25]. Benedetti et al. [26] proposed the critical distance method applied to shot peened fatigue test results, considering the (beneficial) role of the induced residual stress distribution, and for this application the power law relationship was followed too. A different function was implemented by Benedetti et al. [27], still with two parameters again on the shot peening application. On the other hand, by following the inverse search proposed by Santus et al. [22], the length L can be quickly calculated for several values of the number of cycles to failure, thus obtaining an almost continuous function without the need of an interpolating relationship, as discussed by Santus et al. [23].

The TCD is based on a purely elastic material, and this is usually assumed reasonable under the hypothesis of small-scale yielding, in agreement with the linear elastic fracture mechanics. However, a clear definition or standardization of the small-scale yielding limit, applied to the TCD, has been never provided. On the contrary, several attempts have been proposed in the literature aiming at combining the elastic-plastic methodologies and the critical distance, or critical volume, approaches. For example, Benedetti and Santus [28] combined the TCD Point and Line Methods and several multiaxial criteria, showing how the elastic-plastic behavior can play a significant role in particular when the fatigue limit is relatively high with respect to the yield stress. For each of these methods an accurate assessment of the material length should be performed, also evaluating the scatter band for having a statistical significance.

The TCD, under mode I loading and linear elastic material, has been considered for this purpose. After assuming specific probability distributions for the threshold SIF range and the fatigue limit, and introducing these into Eq. (1), the deviation of the critical distance is:

$$L_{th} \pm \delta(L_{th}) = \frac{1}{\pi}\left(\frac{\Delta K_{th} \pm \delta(\Delta K_{th})}{\Delta\sigma_{fl} \pm \delta(\Delta\sigma_{fl})}\right)^2 = L_{th}\left(\frac{1 \pm \delta(\Delta K_{th})/\Delta K_{th}}{1 \pm \delta(\Delta\sigma_{fl})/\Delta\sigma_{fl}}\right) \tag{2a}$$

If the deviations $\delta()$ of the two fatigue properties are small, the first-order approximation can be considered accurate, and the following result is obtained:

$$\delta(L_{th})/L_{th} \approx 2\delta(\Delta K_{th})/\Delta K_{th} + 2\delta(\Delta\sigma_{fl})/\Delta\sigma_{fl} \tag{2b}$$

In other words, the propagation of uncertainty on the critical distance, generated by the ratio of the fatigue properties, is equivalent to the sum of the relative deviations, and the square induces a factor of 2 on both terms.

The strength of a generic (notched) component is then assessed with the TCD by introducing the fatigue limit and this critical distance length, both with their uncertainties:

$$[\Delta\sigma_{fl} \pm \delta(\Delta\sigma_{fl}), L_{th} \pm \delta(L_{th})] \rightarrow \Delta\sigma_{N,fl} \pm \delta(\Delta\sigma_{N,fl}) \quad (3a)$$

When the critical distance is determined by means of a sharp notched specimen, as previously discussed (L value, instead of L_{th}), a different uncertainty is obtained:

$$[\Delta\sigma_{fl} \pm \delta(\Delta\sigma_{fl}), L \pm \delta(L)] \rightarrow \Delta\sigma_{N,fl} \pm \delta'(\Delta\sigma_{N,fl}) \quad (3b)$$

The deviation of L is in principle larger than that of L_{th}, because the crack can be seen as the sharpest notch. This obviously implies that the uncertainty on the estimated strength of the notched component is higher as well:

$$\delta(L) > \delta(L_{th}) \Rightarrow \delta'(\Delta\sigma_{N,fl}) > \delta(\Delta\sigma_{N,fl}) \quad (4)$$

However, for the reasons reviewed above, the threshold data with a sound statistical significance is usually unavailable. Most of the times a similar material is referred and just a single specimen is tested. Therefore, the best strategy is to find the critical distance with a quite sharp notch, and multiple specimens, just disregarding the threshold SIF range, at least obtaining a controlled uncertainty.

The fatigue limit is usually assumed as a Weibull distribution underpinning the "weakest link" damage concept [29, 30, 31]. Nevertheless, for the sake of simplicity, we will assume plain and notch fatigue limit as well as crack threshold to be Gaussian (or *normally*) distributed. In fact, as shown in the following, this assumption permits us to take advantage of recent findings of the statistics research community regarding the distribution of the ratio between two normally distributed variables. We are not aware of similar investigations on differently distributed variables. Moreover, we remind that the very commonly adopted (especially in the industrial field) stair-case procedure assumes the fatigue limit to be normally distributed [32].

As shown in detail below, the obtained distribution of the derived critical distance turns out to be accurately modeled with a *skew-normal* distribution. This statistical analysis was done both for the threshold-derived critical distance, according to Eq. (1), and for the length obtained with the procedure based on the optimized sharp V-notch. The results are compared and discussed and then put into relationship with the local notch radius. Effective and simple fitting equations are then provided to straightforwardly estimate these statistical distributions. These proposed equations are shown in detail in Appendix A, and the procedure can be found as an editable script file for MATLAB® software in Appendix B.

2. Background: inverse determination of the critical length

The procedure recently proposed by Santus et al. [22], for an accurate determination of the critical distance, requires the combined use of the plain specimen and a V-notched cylindrical specimen of

optimal geometry (see Fig. 1a). The critical distance obtained in this way, according to the Line Method (LM), is denoted here as L. The specimen geometry is illustrated in Fig. 1b: A is the notch depth, R is the notch radius, $\bar{\alpha}$ is the notch opening angle and D is the outer diameter of the specimen. The non-dimensional notch depth $A/(D/2) = 0.3$ was selected in [22] to maximize the intensity of the notch tip singular stress term and hence to minimize the sensitivity of the inverse search of critical distance to the experimental uncertainties. In this way, the only independent specimen dimensions are D, R and $\bar{\alpha}$. To keep the problem non-dimensional, the notch root radius, the LM critical distance L and threshold based L_{th} can be normalized with respect to the notch depth and the specimen outer radius, respectively:

$$\rho = \frac{R}{0.3D/2};\ l = \frac{L}{D/2};\ l_{\text{th}} = \frac{L_{\text{th}}}{D/2} \tag{5a}$$

Figure 1c reports the main formulas to obtain l. In brief, the dimensionless critical distance is evaluated from a linear function of the length l_0:

$$l = l_{\min} + \frac{l_0 - \lambda_{\min}}{\varphi} \tag{5b}$$

where l_0 is the critical distance estimated assuming even at the tip of the radiused notch the singular stress distribution reigning in an infinitely sharp notch (see Fig. 1b):

$$\sigma_y(x) = \frac{K_{\text{N}}}{x^s} \tag{5c}$$

In this way l_0 can be expressed as:

$$l_0 = \frac{1}{2}\left(\frac{K_{\text{N,UU}}}{(1-s)K_{\text{f}}}\right)^{1/s};\ K_{\text{N,UU}} = \frac{K_{\text{N}}}{\sigma_{\text{N}}}\frac{1}{\left(D/2\right)^s};\ K_{\text{f}} = \frac{\Delta\sigma_{\text{fl}}}{\Delta\sigma_{\text{N,fl}}} \tag{5d}$$

$K_{\text{N,UU}}$ is the dimensionless (net) Notch Stress Intensity Factor (N- SIF) for unitary nominal stress and unitary scaling length, i.e. when the specimen radius $D/2$ equals unity, and s is the Williams power law singularity exponent. They are reported in Table 1 as a function of two notable values of the notch opening angle $\bar{\alpha}$, viz. 90° and 60°. The fatigue stress concentration factor K_{f}, obtained as the ratio between the fatigue limits of the two specimens, is the only experimental input of the procedure, besides the notched specimen geometry dimensions.

The terms of Eq. (5b) are expressed as a function of the non-dimensional notch radius ρ and the notch opening angle $\bar{\alpha}$ in the following equations:

$$\varphi = \frac{\lambda_{\max} - \lambda_{\min}}{l_{\max} - l_{\min}} \tag{6a}$$

$$l_{\min} = \sum_{i=1}^{4} p_i(\bar{\alpha})\,\rho^{4-i} \tag{6b}$$

$$\lambda_{\min} = \sum_{i=1}^{4} q_i(\bar{\alpha})\,\rho^{4-i} \tag{6c}$$

$$l_{\max} = \lambda_{\max} = c_1(\bar{\alpha}) + c_2(\bar{\alpha})\,\rho^{c_3(\bar{\alpha})} \tag{6d}$$

Best-fit coefficients p_i, q_i, and c_i are reported in Table 2.

The sensitivity analysis conducted in [22] showed that the uncertainty about the estimation of L is the smaller the sharper the radius. In this work, we propose, among other things, to quantify the uncertainty on L based on the statistical dispersion of the fatigue data so as to define the minimum level of sharpness of the notch necessary to bring this uncertainty below a certain threshold.

3. Statistical properties of the critical distance length

3.1 The skew-normal distribution

Looking at the expression of the threshold-derived l_{th} (Eq. (5a)) and notch-derived l (Eq. (5b)) critical distance, it can be noted that both of them are functions of two random variables, viz. $\Delta\sigma_{fl}$, $\Delta\sigma_{N,fl}$ and ΔK_{th}. In general, the statistical distribution of these experimental variables is assumed to be normal, or Gaussian [33]. In this case, according to Eq. (5a), and in turn Eq. (1), and Eq. (5b), l_{th} and l will depend on the ratio between two normal variables. The resulting statistical distribution is still debated in the scientific community [34-37]. It was found that the random variable $Z=X/Y$, being both X and Y normal variables of mean μ_x and μ_y and standard deviation δ_x and δ_y, has no finite moments and its probability distribution function (PDF) is heavy tailed [37,38], yet having a very complicated expression. The shape of this PDF can be uni- or bimodal, asymmetric or symmetric, or even close to a normal distribution, depending fundamentally on the value of the coefficient of variation (CV) of the denominator Y, $r_y = \delta_y/\mu_y$.

Given the though mathematical complexity of this issue, further exacerbated by the elevation to either power 2 or 1/s in Eq. (1) and (5), of the ratio of such normal variables, the only viable approach to this problem is making recourse to a numerical analysis of the statistical distribution of l_{th} and l based on the Monte Carlo (MC) approach. The feasibility of this numerical method is facilitated by the simple mathematical formulation of the inverse procedure of l and l_{th}. In essence, the MC method is based on the generation of a (large) population of individuals through repeated random sampling ("trials"). In each trial, individuals of l_{th} and l data are randomly generated assuming a Gaussian PDF for $\Delta\sigma_{fl}$, $\Delta\sigma_{N,fl}$ and ΔK_{th}. Their mean value and standard deviation will be denoted as $\Delta\bar{\sigma}_{fl}, S, \Delta\bar{\sigma}_{N,fl}, S_N, \Delta\bar{K}_{th}, S_{th}$, respectively. The corresponding CV are defined as follows:

$$r = \frac{S}{\Delta\bar{\sigma}_{fl}};\ r_{th} = \frac{S_{th}}{\Delta\bar{K}_{th}};\ r_N = \frac{S_N}{\Delta\bar{\sigma}_{N,fl}} \tag{7}$$

In the MC simulations, the mean values $\Delta\bar{K}_{th}$ and $\Delta\bar{\sigma}_{N,fl}$ are expressed as a function of an input value $\bar{l}_{th}$ and $\bar{l}$, of l_{th} and l, respectively:

$$\Delta\bar{K}_{th} = \Delta\bar{\sigma}_{fl}\sqrt{\pi\bar{l}_{th}(D/2)};\ \Delta\bar{\sigma}_{N,fl} = \frac{\Delta\bar{\sigma}_{fl}}{K_f(\bar{l})} \tag{8}$$

where the fatigue notch concentration factor K_f is a known function of $\bar{l}$ [22]. It is evident from Eq. (8) that $\bar{l}_{th}$ and $\bar{l}$ represent the critical distances estimated considering the average values $\Delta\bar{\sigma}_{fl}, \Delta\bar{\sigma}_{N,fl}, \Delta\bar{K}_{th}$ of plain and notch fatigue limit as well as crack threshold.

A large number of trials is in general necessary to get stationary statistical properties. A convergence analysis is performed to define a reasonable number of trials. For this purpose, we propose the following index ε expressing the relative fluctuation of a statistical property p:

$$\varepsilon(p) = \frac{\max(p) - \min(p)}{\text{mean}(p)} \tag{9}$$

and apply it to mean, standard deviation and skewness of twenty populations composed of an increasing number of individuals. Looking at Fig. 2, it can be noted that ε asymptotically decreases with the number of trials. The convergence rate is fastest for the mean and lowest for the skewness. In the following, 100,000 trials will be considered, corresponding to a ε value less than 0.1% and 4% for mean and skewness, respectively.

For the moment, we will assume, for the sake of simplicity, that the notch fatigue limit and the crack threshold have the same CV as the plain fatigue limit: $r_{th} = r,\ r_N = r$. The histograms plotted in Figure 3a and b illustrate the PDF of l_{th} and l, respectively, for increasing values of the coefficient of variation r ranging from 0.01 to 0.09. It can be noted that the distribution of both l_{th} and l is unimodal with longer right-sided tail (positive skewness). Its asymmetry becomes more pronounced with increasing r. Interestingly, as long as r is sufficiently small, viz. about 0.07, the PDF histograms are well represented (solid lines) by a skew-normal distribution (SND) expressed as [39]:

$$PDF(x) = \frac{1}{\sqrt{2\pi}\,\gamma}\left(1 + \text{erf}\left(\frac{\alpha(x-\beta)}{\sqrt{2}\,\gamma}\right)\right)\exp\left(-\frac{(x-\beta)^2}{2\gamma^2}\right) \tag{10a}$$

where α, β, and γ are shape, location and scale parameters, respectively. Over other distributions, such as Cauchy, Laplace, Weibull, etc., the SND has the advantage of having the first three moments defined and expressed in the form of algebraic functions of the aforementioned parameters. Indeed, the mean μ, standard deviation δ and skewness sk are respectively given by:

$$\mu = \beta + \frac{\sqrt{\frac{2}{\pi}}\,\alpha\gamma}{\sqrt{1+\alpha^2}} \tag{10b}$$

$$\delta = \gamma\sqrt{1-\frac{2\alpha^2}{\pi(1+\alpha^2)}} \tag{10c}$$

$$sk = \frac{\sqrt{2}(4-\pi)\alpha^3}{\left(\pi+(\pi-2)\alpha^2\right)^{3/2}} \tag{10d}$$

When the shape factor α vanishes, the skewness is zero and the distribution becomes Gaussian of mean β and standard deviation γ. Figure 4a plots the skewness as a function of positive values of α (Eq. (10d)). It can be noted that the skewness is monotonically increasing with α and is bounded from above in the interval [0,1). This means that the SND is suitable to represent populations with low-to-moderate skewness and this is the reason why SND fails to faithfully represent the distribution of l_{th} and l for large values of r: when the skewness approaches the unity (e.g., sk is 0.9 for r = 0.09), α increases asymptotically (see Fig. 4b) leading to the degeneration of the PDF evident in Fig. 3a and b.

The inversion of Eq. (10d) to deduce α from the skewness sk is algebraically though, therefore we propose the following approximate solution:

$$\alpha = \frac{1}{\sqrt{1-sk^2}}\sum_{i=1}^{4} a_i\, sk^{i/2};\ 0 \le sk \le 1 \tag{10e}$$

whose best-fit coefficients a_i are listed in Table 3. As shown in Fig. 4b, the agreement between numerical and analytical solution is very good. Once α has been calculated from Eq. (10e), β and γ can be readily calculated through algebraic solution of Eqs. (10b)-(c).

In the literature, several works [34,38,40] indicate that, as long as the CV of the denominator r_y is sufficiently small (the definition of the upper limit thereof is not unanimous, yet comprised between 0.1 and 1/3), the distribution of the random variable $Z=X/Y$ is reasonably well represented by a normal distribution with mean μ_x/μ_y and CV $\sqrt{r_x^2+r_y^2}$. Since the limit of applicability of the SND to the critical distance is reasonable as long as r is smaller than 0.07, hence within the validity range of the aforementioned calculation of the ratio Z distribution, we propose here to take advantage of this finding to account for values of r_{th} and r_N different from r. The basic idea is to bring this case back to that considered so far (viz. of numerator and denominator of equal CV) by introducing an equivalent CV expressed as:

$$\Sigma_{th} = \sqrt{\frac{r^2+r_{th}^2}{2}};\ \Sigma = \sqrt{\frac{r^2+r_N^2}{2}} \tag{11a}$$

In this way, the resulting approximate normal distribution of the ratios $\Delta K_{th}/\Delta\sigma_{fl}$, $\Delta\sigma_{N,fl}/\Delta\sigma_{fl}$ will have CV equal to $\sqrt{r^2+r_{th}^2}, \sqrt{r^2+r_N^2}$, viz. that expected for numerator and denominator of different CV.

Clearly, this is an approximation, as we already know that the real distribution of l_{th} and l is rather skew-normal than Gaussian. Nevertheless, we found that, as long as the ratio between the CVs is not too far from the unity, this approximation is reasonable. To this regard, let us introduce now an auxiliary coefficient, κ_{th} and κ, expressing the ratio between the CV of numerator and denominator:

$$\kappa_{th} = \frac{r_{th}}{r};\ \kappa = \frac{r_N}{r} \tag{11b}$$

which gives a measure of the deviation from the condition of unitary value under which the approximate distribution of equivalent Σ_{th} and Σ is evaluated.

Figure 5 illustrates the comparison between the actual and the approximate distribution of l_{th} and l in the lower and upper bound of the proposed validity range of this coefficient: $0.5 \le \kappa_{th}, \kappa \le 2.2$. It can be noted that in this interval the approximation is reasonably good. Indeed, the absolute relative difference in standard deviation (and also in CV) is around 3%, whereas that in skewness is up to 50%. This is not surprising as the rationale behind Eq. (11a) is the assumption of a zero-skewness normal distribution. On the other hand, Eq. (11a) allows for a great simplification of the problem of the statistical distribution of l_{th} and l, as the CV will be estimated with a very good approximation only from Σ_{th} and Σ. In essence, this is the greatest advantage of the assumptions of normally distributed input quantities discussed in the Introduction. Conversely, as shown in the next section, mean value and skewness will be expressed as a function of Σ_{th} (or Σ) and κ_{th} (or κ) as well. These statistical properties of l_{th} and l will be investigated through parametric MC simulations.

3.2 Parameters of the skew-normal distribution of l_{th}

The key advantage of introducing the equivalent CV expressed by Eq. (11a) is evident looking at Fig. 6a: when the CV δ_{th}/μ_{th} of the estimation of l_{th} is normalized with respect to Σ_{th} (hereinafter denoted as "normalized CV", NCV), it becomes, with a very good approximation, independent of both Σ_{th} and κ_{th}, therefore well represented by the following expression:

$$\frac{1}{\Sigma_{th}}\frac{\delta_{th}}{\mu_{th}} = \nu_{th} \tag{12a}$$

Importantly, the results of the MC simulations are comprised between an error band estimated with respect to the mean value calculated for κ_{th}=1 (in Fig. 6a and in Eq. (12a) denoted as ν_{th}) that is comprised between -1.0% and 3.5%; moreover, most of the simulations display an absolute error

below 1%. For the purpose of the present work, this accuracy in the estimation of CV is deemed to be adequate. The estimated value of ν_{th}, being approximately equal to 2.8, is listed in Table 4.

Figure 6b illustrates the dependency of the mean to the input value ratio $\mu_{th} / \bar{l}_{th}$ as a function of Σ_{th}, varying parametrically κ_{th}. Interestingly, $\mu_{th} / \bar{l}_{th}$ increases with increasing Σ_{th} and decreasing κ_{th}. We propose here to fit $\mu_{th} / \bar{l}_{th}$ according to the following hyperbolic function:

$$\frac{\mu_{th}}{\bar{l}_{th}} = \cosh\left(\frac{\Sigma_{th}}{m_{th,1} + m_{th,2}\,\kappa_{th}} \right) \tag{12b}$$

Solid curves of Fig. 6b represent the plot of Eq. (12b) with best-fit coefficients $m_{th,i}$ listed in Table 5. From Fig. 6b, it is clear that μ_{th} coincides with $\bar{l}_{th}$ for vanishing Σ_{th} and that μ_{th} progressively deviates from $\bar{l}_{th}$ with increasing Σ_{th}.

A similar behavior is displayed by the skewness sk_{th}, which is plotted in Fig. 6c as a function of Σ_{th}, varying parametrically κ_{th}. For vanishing Σ_{th}, sk tends to zero, while it grows with increasing Σ_{th} and decreasing κ_{th}. A similar hyberbolic function is proposed to fit sk as a function of Σ_{th} and κ_{th}:

$$sk_{th} = \sinh\left(\frac{\Sigma_{th}}{s_{th,1} + s_{th,2}\,\kappa_{th}} \right) \tag{12c}$$

which is represented by solid lines in Fig. 6c and whose best-fit coefficients $s_{th,i}$ are listed in Table 6. Once sk_{th} is determined from Eq. (12c), the shape parameter α of SND can be readily obtained from Eq. (10e), as shown in Fig. 6d. Subsequently, location β and scale γ parameters can be determined from mean (Eq. (12b)) and standard deviation (Eq. (12a)) by algebraic solution of Eqs. (10b) and (10c).

3.3 Parameters of the skew-normal distribution of l

On the base of the sensitivity analyses carried out in [22] on the inverse determination of notch-derived critical distance l, we can already anticipate that its statistical distribution shall be strongly correlated to the notch radius of the notched specimen used to determine K_f. To this regard, Fig. 7a shows the results of MC simulations carried out to explore the dependency of the NCV, $\delta / (\Sigma\,\mu)$, upon the input crack length $\bar{l}$ taking the notch radius ρ as a parameter. Importantly, CV declines asymptotically with increasing $\bar{l}$ and gets larger with increasing ρ. Moreover, the asymptotic value (black dashed line in Fig. 7a), here denoted as ν_s and compared in Table 4 with ν_{th} for two opening angles $\bar{\alpha}$ (90° and 60°), corresponds to the condition of infinitely sharp notch ($\rho = 0$). This value is

obtained from MC simulations considering the singular stress field expressed by Eq. (5c) and, similarly to $\overline{l}_{\text{th}}$, is independent of the critical distance $\overline{l}$.

It is now clear that, in contrast to l_{th}, the statistical distribution of l will depend on an additional geometric parameter, namely the notch radius ρ. Accordingly, we expect that NCV will increase with declining stress gradient ahead of the radiused notch tip, which in turn is inversely proportional to the notch radius ρ. Consequently, NCV is an increasing function of ρ that is bounded from below by ν_0. To eliminate the dependency upon ρ, we propose here to research the *locus* of points satisfying the following equality:

$$\frac{1}{\Sigma}\frac{\delta}{\mu} = \nu;\ \nu_0(\bar{\alpha}) \le \nu \le 7 \Rightarrow \overline{l} = l_{\text{lim}} \tag{13a}$$

where the parameter ν is a constant comprised between ν_0 and 7. This upper bound was selected after realizing that even larger values of ν lead to excessively dispersed distributions of l hardly representable by a SND. Figure 7b gives an illustrative example of this *locus* when the parameter ν is equal to 5. Dotted values are obtained by numerically searching the intersection of families of curves similar to those plotted in Fig. 7a with the horizontal line ν = constant. The equivalent CV Σ and the notch radius ρ are varied parametrically, while keeping fixed the notch angle $\bar{\alpha}$ and κ (=1). Importantly, the *locus* of $\overline{l}$ is found to be independent of Σ and an increasing function of ρ. Within the validity range of the inverse search function ($l_{\text{min}} \le \overline{l} \le l_{\text{max}}$), this *locus* of $\overline{l}$, here denoted as l_{lim}, is well represented by the following quadratic polynomial:

$$l_{\text{lim}} = b_1(\bar{\alpha},\nu)\,\rho + b_2(\bar{\alpha},\nu)\,\rho^2 \tag{13b}$$

where the coefficients b_i are function of $\bar{\alpha}$ and ν and their best-fit values are listed in Table 7.

It is now clear that values of $\overline{l}$ satisfying Eq. (13b) are characterized by a NCV equal to ν with a degree of approximation that can be deduced from Fig. 7c. For the explored values of the notch radius ρ, the NCV value is approximated by that predicted by Eq. (13a) with an absolute error below 1.5%. Equation (13b) can be easily inverted to determine the value ρ_{lim} of the notch radius ρ that makes the NCV of the estimation of $\overline{l}$ equal to ν:

$$\rho_{\text{lim}} = \frac{-b_1(\bar{\alpha},\nu) + \sqrt{b_1(\bar{\alpha},\nu)^2 + 4b_2(\bar{\alpha},\nu)\,\overline{l}}}{2b_2(\bar{\alpha},\nu)};\ R_{\text{lim}} = 0.3\frac{D}{2}\rho_{\text{lim}} \tag{13c}$$

In the following, the statistical properties of l will be analyzed by exploring parametrically five values of ν, namely ν_0, 4, 5, 6, 7. This permits to build the plot reported in Fig. 7d, where the dotted values represent, for parametrically varying $\overline{l}$, the value ν corresponding to a certain notch radius ρ. Interestingly, the family of curves, parametric in $\overline{l}$, converges for $\rho = 0$ (infinitely sharp notch) to

the same value ν_0. Moreover, with increasing ρ, the increment in NCV is particularly pronounced for small values of $\bar{l}$. The dotted values of Fig. 7d are interpolated with good accuracy by the following expression (solid lines):

$$\nu = \nu_0 + n_1(\bar{\alpha})\frac{\rho}{\bar{l}^{\,n_3(\bar{\alpha})}} + n_2(\bar{\alpha})\frac{\rho^2}{\bar{l}^{\,n_4(\bar{\alpha})}} \tag{13d}$$

Best-fit coefficients n_i are listed in Table 4 for two values of $\bar{\alpha}$.

Eq. (13d) and Figure 7c are of particular interest, mainly for two reasons: (i) given the input value $\bar{l}$ and the notch radius of the specimen used to deduce l, the expected NCV for the estimation of l can be readily calculated from Eq. (13d); (ii) when designing the notched specimen geometry for the experimental evaluation of l, the designer can assess, from the expected value of $\bar{l}$, the notch radius necessary to bring the NCV of l equal to the desired level ν.

The knowledge of ν through Eq. (13d) is also useful to infer the statistical properties of l. Indeed, the CV can be immediately deduced from Eq. (13a), while the equations derived in the following for estimating mean and skewness for five discrete values of ν (ν_0, 4, 5, 6, 7), can be extended to intermediate ν values through simple interpolation.

Figure 8a illustrates the results of MC simulations showing that Eq. (13a) is able to accurately predict the value of NVC for any values of Σ and κ comprised within the validity range: the corresponding relative error is comprised between -1.0% and +2.5%. Figure 7b shows the results of MC simulations demonstrating that the average value of l satisfying Eq. (13b) are very little affected by the notch radius ρ. We come to similar conclusions (here not reported for the sake of brevity) also for the skewness sk. Therefore, in the following, mean and skewness corresponding to a certain combinations of Σ and κ will be evaluated by averaging the values obtained for all the explored valus of ρ. These averaged values are shown in Fig. 8c and 8d for mean and skewness, respectively. The obtained trends are very similar to those found for l_{th}. Therefore, we propose to interpolate them with formally identical expressions suggested for mean value:

$$\frac{\mu}{\bar{l}} = \cosh\left(\frac{\Sigma}{m_1(\bar{\alpha},\nu) + m_2(\bar{\alpha},\nu)\kappa}\right) \tag{13e}$$

and skewness:

$$sk = \sinh\left(\frac{\Sigma}{s_1(\bar{\alpha},\nu) + s_2(\bar{\alpha},\nu)\kappa}\right) \tag{13f}$$

Best-fit coefficients m_i and s_i of Eqs. (13e) and (13f) are listed in Tables 5 and 6, respectively, for different values of ν and $\bar{\alpha}$. Parametric plots of of Eqs. (13e) and (13f) are provided in Fig. 8c and 8d, respectively. Interestigly, looking at the best-fit coefficients s_i listed in Table 6, it can be noted

that the skewness is very weakly dependent on ν. A very small estimation error (relative absolute error below 1%) is made when replacing the coefficients listed in Table 6 for different ν by average values.

Again, once *sk* is determined from Eq. (13f), the shape parameter α of SND can be readily obtained from Eq. (10e). Subsequently, location β and scale γ parameters can be determined from mean (Eq. (13e) interpolated at the corresponding value of ν given by Eq. (13d)) and standard deviation (Eq. (13a) and (13d)) by algebraic solution of Eqs. (10b) and (10c).

To conclude, Table 8 summarizes the validity range under which the proposed method to deduce the statistical properties of l_{th} and l can be used with adequate level of approximation. The proposed method permits to determine mean, standard deviation and skewness of the statistical distribution of l_{th} and l as a function of Σ (or Σ_{th}), κ (or κ_{th}), ρ, and $\bar{\alpha}$. The *modus operandi* for determining the statistical properties of l_{th} and l is illustrated by the flow-chart reported in Fig. 9 and implemented in Matlab scripts enclosed in the electronic version of the paper and described in the Appendix. The designer can incorporate this information into a probabilistic fatigue calculation of notched components. In the next section, we will show how the statistical distribution of l_{th} and l affects the fatigue strength of notched specimens of the same geometry depicted in Fig. 1, yet of different notch angle $\bar{\alpha}$ and notch radius ρ from those of the notched specimen used to determine the critical length.

3.4 Effect of the statistical distribution of l_{th} and l on the predictions of the Line Method

MC simulations are run according to the following steps:

1. Extraction of l_{th} or l from a skew-normally distributed population with parameters expressed by Eqs. (12) or (13) as a function of Σ (or Σ_{th}), κ (or κ_{th}), ν, and $\bar{\alpha}$.
2. Calculation of the corresponding value of K_f.
3. Calculation of the notched fatigue strength $\Delta\sigma_{N,fl}$ from K_f and the plain fatigue limit extracted from a normally distributed population of mean $\Delta\bar{\sigma}_{fl}$ and CV: $\frac{S}{\Delta\bar{\sigma}_{fl}} = \begin{cases} \frac{\Sigma}{\sqrt{\frac{1+\kappa^2}{2}}} \\ \frac{\Sigma_{th}}{\sqrt{\frac{1+\kappa_{th}^2}{2}}} \end{cases}$
4. Calculation of the NCV of $\Delta\sigma_{N,fl}$.

The results of the MC simulations (dotted values) are shown in Fig. 10a and 10c for the NCV of the prediction of $\Delta\sigma_{N,fl}$ starting from l_{th} or l, respectively, in the case of infinitely sharp notch (ρ = 0). It can be noted that NCV is higher for the lowest value for explored interval of κ and κ_{th} (=0.5). In order

to eliminate the dependency upon this parameter, we propose here to investigate the NCV of $\Delta\sigma_{N,fl}$ for radiused notches considering, for the sake of conservatorism, the value of κ and κ_{th} (=0.5) leading to the largest dispersion of notch fatigue strength predictions. Moreover, it can be noted that NCV is practically independent of Σ_{th}, while it tends to decline for large values of Σ. For this reason, again for the sake of conservatorism, the following plots will be displayed and analysed for $\Sigma_{th}=\Sigma=1/100$ and $\kappa_{th} = \kappa = 0.5$, as they were found to give the largest values of NCV.

The results of the MC simulations (dotted values) are shown in Fig. 10b and 10d for the NCV of $\Delta\sigma_{N,fl}$ for radiused notches, exploring parametrically the critical distance l_{th} or l, respectively. Interestingly, NCV declines with decreasing sharpness (increasing ρ) of the notch and gets higher with increasing $\overline{l}_{th}$ or $\overline{l}$. In other words, the uncertainty about the notch fatigue limit is higher the greater the critical length with respect to the notch radius. Furthermore, the trends converge to the same CV value for the infinitely sharp notch ($\rho = 0$) regardless of the $\overline{l}_{th}$ or $\overline{l}$ value.

The dotted values of Fig. 10b and 10d are very well represented by the solid lines expressed by the following bivariate function of ρ and $\overline{l}_{th}$ or $\overline{l}$, respectively:

$$\frac{1}{\Sigma_{th}}\frac{S_N}{\Delta\bar{\sigma}_{N,fl}} = f_{th,1} + \frac{1}{f_{th,2} + f_{th,3}\dfrac{\rho}{\overline{l}_{th}^{\,f_{th,5}}} + f_{th,4}\dfrac{\rho^2}{\overline{l}_{th}^{\,f_{th,6}}}} \tag{14a}$$

$$\frac{1}{\Sigma}\frac{S_N}{\Delta\bar{\sigma}_{N,fl}} = f_1(\bar{\alpha},\nu) + \frac{1}{f_2(\bar{\alpha},\nu) + f_3(\bar{\alpha},\nu)\dfrac{\rho}{\overline{l}^{\,f_5(\bar{\alpha},\nu)}} + f_4(\bar{\alpha},\nu)\dfrac{\rho^2}{\overline{l}^{\,f_6(\bar{\alpha},\nu)}}} \tag{14b}$$

Best-fit coefficients $f_{th,i}$ and f_i of Eq. (14a-b) are listed in Table 9 for different values of ν and $\bar{\alpha}$. In essence, Eqs. (14a) and (14b) permit to calculate the NCV of the estimation of the fatigue limit of any notched specimen geometry, including the infinitely sharp one.

Similar MC simulations are carried out to determine the NCV of the estimation of the crack growth treshold ΔK_{th} from l_{th} or l (skew-normally distributed) and $\Delta\sigma_{fl}$ (normally distributed) and their results are shown in Fig. 11a and 11b, respectively, for different values of Σ (or Σ_{th}) and κ (or κ_{th}). Clearly, it makes no sense to estimate ΔK_{th} from l_{th}, as this latter value requires the knowledge of ΔK_{th}. Nevertheless, the comparison of the NCV obtained in both ways is interesting for assessing the effect of the larger dispersion of l with respect of l_{th} on the estimation of ΔK_{th}. From Fig. 11a and b, it can be noted that the largest NCV in the estimation of ΔK_{th} is obtained for $\kappa_{th} = \kappa = 0.5$. This value is used to give an upper bound (solid lines in Fig. 11a and b) of the NCV and expressed by the following equations:

$$\frac{1}{\Sigma_{th}}\frac{S_{th}}{\Delta\bar{K}_{th}} = d_{th} \quad (15a)$$

$$\frac{1}{\Sigma}\frac{S_{th}}{\Delta\bar{K}_{th}} = d(\nu) \quad (15b)$$

Best-fit coefficients d_{th} and d of Eq. (15a-b) are listed in Table 10 for different values of ν.

4. Applicative examples

4.1 Experimental data

In this section, we will use the experimental data that were collected in [23] to test the inverse search procedure of the critical length devised in [22]. The purpose is to characterize the stochastic properties of l_{th} and l and their effect on the prediction of independent experimental fatigue data. Specifically, plain, notched and fracture mechanics specimens were extracted from bars of aeronautical aluminum grade 7075-T6 and steel 42CrMo4+QT (quenched and tempered). Details regarding the material and experimental procedures used to generate the fatigue data analyzed in this article can be found in [23].

In [23] the fatigue characterization was carried out under fully-reversed (load ratio R = −1) and pulsating (R = 0.1) axial fatigue on axisymmetric plain and V-notched samples, whose geometries are shown in Fig. 12. The outcomes of the fatigue tests carried out on the plain samples are listed in Table 11 in terms of average stress amplitude and standard deviation on the stress amplitude evaluated in the high-cycle fatigue regime.

Notches of different severity were explored by changing the notch root radius R (see Fig. 1a and c). In the sharp and blunt notch configuration, R is set equal to 0.2 mm (effective size measured by SEM is 0.21 mm, theoretical principal stress concentration factor K_t = 5.75) and 1 mm (K_t = 2.88), respectively. In [41] a third notched geometry, termed ultra-sharp, wherein R is 0.1 mm (effective size 0.12 mm, K_t = 7.42) was investigated with the aim of exploring the effect of an even sharper notch geometry. The experimentation was complemented in [23] by fatigue crack growth tests conducted at R = −1 and R = 0.1 using C(T) and M(T) specimens, respectively, also shown in Fig. 12. The outcomes in terms of crack threshold ΔK_{th} are listed in Table 12. In contrast to plain and notch fatigue strength data, no information is available about the standard deviation on ΔK_{th}, as only a single test was performed per each experimental variant. In order to simulate the stochastic variability of ΔK_{th}, we will assume in the present case that the mean value corresponds to the experimental value. The standard deviation is here inferred from [42] where the scatter band of fatigue crack growth curves of 7075-T651 was estimated on the basis of six tests undertaken on three different material lots. The tests showed that the corresponding crack growth threshold ΔK_{th} at R =

0.1 was between 2.1 and 2.8 $\mathrm{MPa}\sqrt{\mathrm{m}}$. Assuming these data normally distributed and comprised in the band $\pm 2S_{th}$ (95% probability), S_{th} is then estimated to be about 0.18 $\mathrm{MPa}\sqrt{\mathrm{m}}$. The standard deviation of the remaining experimental variants listed in Table 12 are scaled according to the ratio between mean values of ΔK_{th}. In [43], the same notched specimen geometry was used to determine the critical distance in additively manufactured Ti-6Al-4V. Unfortunately, the obtained results are here not discussed as their statistical properties do not satisfy the validity conditions set by Table 8.

4.2 Statistical distribution of l_{th} and l

Table 12 lists also the statistical properties of threshold-derived critical length l_{th}. These are estimated using both Eqs. (12a-c) and MC simulations where, during each trial, l_{th} is computed extracting normally distributed values of plain fatigue limit and crack threshold with mean and standard deviation listed in Table 11 and 12. The agreement among the statistical parameters estimated in the two ways is very good. Data referred to 42CrMo4+QT tested at R=0.1 are shown in bold because the ratio $\kappa_{th} = r_{th}/r$ lies outside the validity range shown in Table 8 and will be therefore ruled out in the rest of the discussion.

Figure 13a and 13b compare the PDF of L_{th} estimated through MC simulations (histograms) and the SND with parameters deduced from Eqs. (12) and listed in Table 10 (solid curves) for 7075-T6 tested under R = −1 and R = 0.1, respectively. The agreement between the two approaches is pretty good, especially for R = −1. Conversely, despite the very good agreement of the predictions made by Eqs. (12) in terms of mean, standard deviation and skewness with MC simulations, the agreement between predicted PDF and histogram for R = 0.1 is less good (Fig. 13b), especially for the left tail of the distribution. This can be imputed to the slight violation on the maximum limit set on Σ_{th} (mainly due the highly dispersed plain fatigue limit), that makes the statistical distribution less accurately represented by a SND.

The threshold-derived critical length estimations L_{th} can be now used to infer from Eq. (13d) the NCV value expected for the notch-derived estimations l. This scenario is illustrated in Fig. 13c for 7075-T6. Interestingly, when l is deduced from ultra-sharp notched specimens NCV is comprised between 4.3 and 4.9, while when it is obtained from sharp notched specimens NCV increases up to 5.2 and 6.2, respectively. This result outlines the fundamental role played by small values of ρ to get l estimations affected by low standard deviation.

Table 13 lists the experimental results of the fatigue tests carried out on the sharp and ultra-sharp notched specimens used to deduce the critical length l. In all the experimental variants, the conditions set in Table 8 on Σ and κ are satisfied. For 7075-T6, NCV is very similar to that anticipated in Fig. 13c using threshold-derived critical distance estimations, being comprised between 4.4 and 6.6. For

42CrMo4+QT, wherein only sharp notched specimens were used, NCV is higher, namely comprised between 6.2 and 7.3. The latter value is slightly higher than the maximum allowable value set in Table 8 equal to 7, yet considered still acceptable for a proper statistical characterization. To determine the statistical properties of l estimations affected by these NCV values, the results of Eqs. (13) for discrete ν values are interpolated at the effective ν value of each experimental variants. Importantly, the relative absolute error made in the estimation of mean, standard deviation and skewness is below 2% in all the investigated experimental variants. Such good agreement is also evident looking at Fig. 14a-d, which compare the PDF of L estimated through MC simulations (histograms) and the SND with parameters deduced from Eqs. (13) and listed in Table 13 for 7075-T6 tested under R = −1 and R = 0.1 using both ultra-sharp and sharp notched specimens. Interestingly, comparing Fig. 13a-b and 14a-d, it can be noted that the peak of the statistical distribution progressively declines passing from the fracture mechanics to the notched specimen with decreasing sharpness of the notch root as a consequence of the concomitant increment in NCV ν. On the other hand, a notch-derived critical length estimation allows for a simpler and sounder statistical characterization, as the standard deviation of the notch fatigue limit can be quantified with a much lesser experimental effort as compared to the crack threshold. Furthermore, if a notched specimen geometry of adequate sharpness is adopted, the increment in standard deviation can be kept small (compare Table 12 and 13).

4.3 Prediction of the fatigue limit of independent experimental variants

Table 14 and 15 list the predictions of the notch fatigue strength and crack growth threshold of variants not used to determine l_{th} and l, respectively. In this case as well, the predictions are made through MC simulations and according to the simplified approach expressed by Eqs. (14) and (15) for the CV, while the mean value is calculated starting from the mean plain fatigue limit $\Delta\bar{\sigma}_{fl}$ and the mean value of the critical length μ_{th} (Eq. (12b)) and μ (Eq. (13e)). The agreement between the two approaches is very good: the mean value is almost identical; the standard deviation is always slightly overestimated by the simplified method (see conservative assumptions taken in Section 3.4) with respect to MC simulations. The simplified method overestimates, even though to a reasonably extent, the standard deviation with respect to the experimental value; hence, the method here adopted for its derivation can be profitably exploited in any reliability-based fatigue design approach. To conclude, it can be noted that the LM is less accurate in predicting the fatigue limit of the independent experimental variants of steel 42CrMo4+QT as compared with 7075-T6: this issue was already discussed in our previous works [28, 41] and mainly attributed to plasticity effects that are not captured by a pure linear-elastic formulation of TCD.

5. Conclusions

The present paper investigated the statistical properties of the critical distance estimations obtained from crack threshold (l_{th}) or notch fatigue limit (l). The latter estimation is based on an inverse search procedure proposed in [22] that requires a specific notch geometry devised to minimize the sensitivity of l to the experimental uncertainty. It was found that, if the input quantities are normally distributed, the output variable has a non-symmetric probability density function that, under certain conditions, is well represented by a skew normal distribution. Approximate functions were proposed to predict mean, standard deviation and skewness of such distribution and tested using real experimental data. The following conclusions can be drawn:

1) The cracked specimen geometry permits to estimate l_{th} with the lowest possible normalized coefficient of variation (NCV). The notch-derived l estimation is affected by larger NCV, which increases with increasing notch radius. In this case, NCV depends on the notch radius ρ and opening angle $\bar{\alpha}$ only (Eq. (12d)). This makes it possible to design *a priori* the notch specimen geometry according to the desired NCV of l estimation.
2) The notch radius of the notched specimen geometry used for the inverse search of the critical distance l is the key geometrical parameter controlling the dispersion and therefore the uncertainty about l. The smallest dispersion is ensured by the inverse search from the crack threshold, whose experimental evaluation is however much more challenging with respect to the notch fatigue limit, especially if replicated fracture mechanics tests must be carried out to estimate its standard deviation.
3) The statistical properties of l and l_{th} can be used to estimate the dispersion of the predictions of independent notched or cracked geometries. The dispersion increases with increasing sharpness of the notch to be assessed (being the cracked configuration the sharpest notch possible) and with rising non-dimensional critical length.
4) A rapid estimation of the statistical properties of l and l_{th} (mean, standard deviation and skewness) is made possible by MATLAB scripts attached to the on-line version of the paper.

Appendix A

A calculation example is reported in this appendix, showing step-by-step the proposed procedure. The data reported here is referring to the experimental results of Aluminum alloy 7075-T6 and load ratio R = –1, comparing the critical distance distribution data as predicted with the ultra-sharp specimen and the threshold. This calculation sequence follows the flowchart illustrated in Fig. 9, and can also be retrieved in the editable script file for MATLAB® software, available online in Appendix

B. The material data considered, both as input of the procedure and results, can be found in Tables 11-15.

The following basic fatigue strength properties are introduced. The plain specimen:

$$\Delta\bar{\sigma}_{\mathrm{fl}}/2 = 159\,\mathrm{MPa},\ S/2 = 5.23\,\mathrm{MPa} \tag{A.1a}$$

the ultra-sharp specimen, $\bar{\alpha} = 90°, R = 0.12\,\mathrm{mm}$:

$$\Delta\bar{\sigma}_{\mathrm{fl}}/2 = 38.2\,\mathrm{MPa},\ S_{\mathrm{N}}/2 = 2.19\,\mathrm{MPa} \tag{A.1b}$$

and the threshold SIF range, obtained with the M(T) specimen:

$$\Delta\bar{K}_{\mathrm{th}} = 4.2\,\mathrm{MPa}\sqrt{\mathrm{m}},\ S_{\mathrm{th}}/2 = 0.30\,\mathrm{MPa}\sqrt{\mathrm{m}} \tag{A.1c}$$

The plain and the notched specimen data can be combined, obviously to find the fatigue stress concentration factor, along with the coefficients of variation and the equivalent CV:

$$K_{\mathrm{f}} = 4.162 \tag{A.2a}$$

$$r = 0.03289 \tag{A.2b}$$

$$r_{\mathrm{N}} = 0.05733 \tag{A.2c}$$

$$\kappa = 1.743 \tag{A.2d}$$

$$\Sigma = 0.04674 \tag{A.2e}$$

The dimensionless LM critical distance length, obtained from the inverse search procedure, results:

$$\bar{l} = 0.00520 \tag{A.3a}$$

and the dimensional critical distance is ($D = 20\,\mathrm{mm}$):

$$\bar{L} = 0.0520\,\mathrm{mm} \tag{A.3b}$$

The normalized CV can be obtained from Eq. (13d):

$$\nu = 4.368 \tag{A.4}$$

and the mean (dimensionless) critical distance μ can be obtained by interpolating Eq. (13e). Specific values of ν are considered, namely: $\nu = \nu_0, 4, 5, 6, 7$ for which the m_1, m_2 values are avalable, as reported in Table 5. The mean value of μ is calculated for these values:

$$\mu(\nu) = \bar{l}\cosh\left(\frac{\Sigma}{m_1(\bar{\alpha},\nu) + m_2(\bar{\alpha},\nu)\kappa}\right),\ \nu = \nu_0, ..., 7 \tag{A.5a}$$

and then by piecewise linear interpolation it follows:

$$\mu(\nu = 4.368) = 0.00526 \tag{A.5b}$$

A similar procedure is followed to find the skewness of the distribution, according to Eq. (13f), and again interpolating according to the NCV, the following result is obtained:

$$sk(\nu) = \sinh\left(\frac{\Sigma}{s_1(\bar{\alpha},\nu) + s_2(\bar{\alpha},\nu)\,\kappa}\right),\ sk(\nu = 4.368) = 0.3406 \tag{A.6}$$

The standard deviation can be found by inverting Eq. (13a):

$$\delta = \nu\,\mu\,\Sigma = 0.001075 \tag{A.7}$$

and the shape parameter α of the distribution can be obtained with Eq. (10e):

$$\alpha = 1.635 \tag{A.8}$$

Now the scale parameter λ can be found by inverting Eq. (10c) since the values δ, α are available:

$$\gamma = \frac{\delta}{\sqrt{1 - \frac{2\alpha^2}{\pi(1+\alpha^2)}}} = 0.001467 \tag{A.9}$$

and the location parameter β is obtained with Eq. (10b):

$$\beta = \mu - \frac{\sqrt{\frac{2}{\pi}}\,\alpha\,\gamma}{\sqrt{1+\alpha^2}} = 0.004266 \tag{A.10}$$

All the parameters for the skew-normal PDF distribution are available at this point, which can be introduced into Eq. (10a).

The skew-normal distribution of the threshold-derived critical distance can be calculated by following similar steps, as in the workflow shown in Fig. 9. By combing the experimental threshold SIF range, recalled in Eq. (A.1c), and the plain specimen fatigue limit Eq. (A.1a), the obtained critical distance is:

$$\bar{L}_{\text{th}} = 0.0555\,\text{mm} \tag{A.11a}$$

$$\bar{l}_{\text{th}} = \bar{L}_{\text{th}} / (D/2) = 0.00555 \tag{A.11b}$$

Along with the following coefficient of variation and equivalent CV based on the threshold determination:

$$r_{\text{th}} = 0.07143 \tag{A.12a}$$

$$\kappa_{\text{th}} = 2.172 \tag{A.12b}$$

$$\Sigma_{\text{th}} = 0.05561 \tag{A.12c}$$

while the NCV is a fixed value:

$$\nu_{\text{th}} = 2.842 \tag{A.13}$$

From Eqs. (12b) and (12c) the mean value and the skewness can be found:

$$\mu_{\text{th}} = 0.00560 \tag{A.14}$$

$$sk_{\text{th}} = 0.3177 \quad \text{(A.15)}$$

Similarly to above, the standard deviation is retrieved with Eq. (12a):

$$\delta_{\text{th}} = 0.0008843 \quad \text{(A.16)}$$

and by following the same steps all the other parameters of the PDF are obtained:

$$\alpha_{\text{th}} = 1.570 \quad \text{(A.17)}$$

$$\gamma_{\text{th}} = 0.001196 \quad \text{(A.18)}$$

$$\beta_{\text{th}} = 0.004791 \quad \text{(A.19)}$$

The strength of a blunter notch (R = 1.0 mm) is assessed, both with $\bar{L}_{\text{th}}$ and $\bar{L}$ considering their statistical distributions. By inverting Eq. (5b) with $l = \mu_{\text{th}}$ as input, l_0 is found. K_{f} is then obtained with the first of Eq. 5(d) inverted, and the fatigue limit of the notched specimen is:

$$\mu_{\text{th}} \rightarrow \Delta\bar{\sigma}_{\text{N,fl}} / 2 = 62.0\,\text{MPa} \quad \text{(A.20a)}$$

The standard deviation of this value is obtained with Eq. (14a):

$$S_{\text{N}} / 2 = 4.47\,\text{MPa} \quad \text{(A.20b)}$$

This fatigue limit can be similarly obtained with the mean value of the LM critical distance, μ, by following the same steps, i.e. by inverting Eqs. (5):

$$\mu \rightarrow \Delta\bar{\sigma}_{\text{N,fl}} / 2 = 61.6\,\text{MPa} \quad \text{(A.21a)}$$

Eq. (14b) can be used for the standard deviation, however, an interpolation in terms of the CV is required:

$$\nu = 4.368 \rightarrow S_{\text{N}} / 2 = 3.84\,\text{MPa} \quad \text{(A.21b)}$$

The threshold SIF range can be assessed with the dimensional mean value of the critical distance, using Eq. (8) in which the length $\mu(D/2)$ is introduced. The result obtained is:

$$\Delta K_{\text{th}} = 4.09\,\text{MPa}\sqrt{\text{m}} \quad \text{(A.22a)}$$

and the standard deviation is given by Eq. (15b), after interpolating again with respect to ν:

$$S_{\text{th}} = 0.48\,\text{MPa}\sqrt{\text{m}} \quad \text{(A.22b)}$$

References

[1] D. Taylor, The Theory of Critical Distances: A New Perspective in Fracture Mechanics, Elsevier Science, 2007, ISBN: 9780080444789.

[2] L. Susmel, D. Taylor, A critical distance/plane method to estimate finite life of notched components under variable amplitude uniaxial/multiaxial fatigue loading, International Journal of Fatigue 38 (2012) 7–24. doi:10.1016/j.ijfatigue.2011.11.015.

[3] D. Liao, S.-P. Zhu, G. Qian, Multiaxial fatigue analysis of notched components using combined critical plane and critical distance approach, International Journal of Mechanical Sciences 160 (2019) 38–50. doi:10.1016/j.ijmecsci.2019.06.027.

[4] C. Santus, Initial orientation of the fretting fatigue cracks in shrink-fit connection specimens, Frattura ed Integrità Strutturale 13 (48) (2019) 442–450. doi:10.3221/IGF-ESIS.48.42.

[5] ASTM, Test Method for Measurement of Fatigue Crack Growth Rates, ASTM E647-15e1 (2015). doi:10.1520/e0647-15e01.

[6] S. C. Forth, J. C. J. Newman, R. G. Forman, On generating fatigue crack growth thresholds, International Journal of Fatigue 25 (1) (2003) 9–15. doi:10.1016/S0142-1123(02)00066-X.

[7] J. B. Jordon, J. C. J. Newman, Y. Xue, M. F. Horstemeyer, Near threshold fatigue crack growth in 7075-T651 aluminum alloys, in: Proceedings of the 2006 SEM Annual Conference & Exposition on Experimental & Applied Mechanics: June 4-7, 2006, Saint Louis, Missouri, USA, 2006, pp. 1–9, ISBN 091205395X.

[8] J. C. Newman, Y. Yamada, Compression precracking methods to generate near-threshold fatigue-crack-growth-rate data, International Journal of Fatigue 32 (6) (2010) 879–885. doi:10.1016/j.ijfatigue.2009.02.030.

[9] U. Zerbst, M. Vormwald, R. Pippan, H.-P. Gänser, C. Sarrazin-Baudoux, M. Madia, About the fatigue crack propagation threshold of metals as a design criterion – A review, Engineering Fracture Mechanics 153 (2016) 190–243. doi:10.1016/j.engfracmech.2015.12.002.

[10] U. Zerbst, M. Madia, M. Vormwald, Applying fracture mechanics to fatigue strength determination – Some basic considerations, International Journal of Fatigue 126 (2019) 188–201. doi:10.1016/j.ijfatigue.2019.05.009.

[11] A. H. Noroozi, G. Glinka, S. Lambert, Prediction of fatigue crack growth under constant amplitude loading and a single overload based on elasto-plastic crack tip stresses and strains, Engineering Fracture Mechanics 75 (2) (2008) 188–206. doi:10.1016/j.engfracmech.2007.03.024.

[12] L. Susmel, D. Taylor, The Theory of Critical Distances as an alternative experimental strategy for the determination of KIc and DKth, Engineering Fracture Mechanics 77 (9) (2010) 1492–1501. doi:10.1016/j.engfracmech.2010.04.016.

[13] D. Taylor, Applications of the theory of critical distances in failure analysis, Engineering Failure Analysis 18 (2) (2011) 543–549. doi:10.1016/j.engfailanal.2010.07.002.

[14] L. Susmel, D. Taylor, A novel formulation of the theory of critical distances to estimate lifetime of notched components in the medium-cycle fatigue regime, Fatigue and Fracture of Engineering Materials and Structures 30 (7) (2007) 567–581. doi:10.1111/j.1460-2695.2007.01122.x.

[15] L. Susmel, D. Taylor, The theory of critical distances to predict static strength of notched brittle components subjected to mixed-mode loading, Engineering Fracture Mechanics 75 (3-4) (2008) 534–550. doi:10.1016/j.engfracmech.2007.03.035.

[16] S. Cicero, V. Madrazo, I. A. Carrascal, On the Point Method load-bearing capacity predictions in Al7075-T651 structural components containing stress risers, Engineering Failure Analysis 26 (2012) 129–138. doi:10.1016/j.engfailanal.2012.07.008.

[17] S. Cicero, V. Madrazo, T. García, Analysis of notch effect in the apparent fracture toughness and the fracture micromechanisms of ferritic–pearlitic steels operating within their lower shelf, Engineering Failure Analysis 36 (2014) 322–342. doi:10.1016/j.engfailanal.2013.10.021.

[18] T. Yin, A. Tyas, O. Plekhov, A. Terekhina, L. Susmel, A novel reformulation of the Theory of Critical Distances to design notched metals against dynamic loading, Materials and Design 69 (2015) 197–212. doi:10.1016/j.matdes.2014.12.026.

[19] W. Li, L. Susmel, H. Askes, F. Liao, T. Zhou, Assessing the integrity of steel structural components with stress raisers using the Theory of Critical Distances, Engineering Failure Analysis 70 (2016) 73–89. doi:10.1016/j.engfailanal.2016.07.007.

[20] W. Li, H. Askes, L. Susmel, Notch failure versus interior failure for mixed-mode in-plane loading, International Journal of Solids and Structures 150 (2018) 208–221. doi:10.1016/j.ijsolstr.2018.06.014.

[21] S. Cicero, P. González, B. Arroyo, J. A. Álvarez, Analysis of environmentally assisted cracking processes in notched steels using the point method, Procedia Structural Integrity 18 (2019) 3–11. doi:10.1016/j.prostr.2019.08.134.

[22] C. Santus, D. Taylor, M. Benedetti, Determination of the fatigue critical distance according to the Line and the Point Methods with rounded V-notched specimen, International Journal of Fatigue 106 (2018) 208–218. doi:10.1016/j.ijfatigue.2017.10.002.

[23] C. Santus, D. Taylor, M. Benedetti, Experimental determination and sensitivity analysis of the fatigue critical distance obtained with rounded V-notched specimens, International Journal of Fatigue 113 (2018) 113–125. doi:10.1016/j.ijfatigue.2018.03.037.

[24] R. Negru, D. A. Serban, L. Marsavina, A. Magda, Lifetime prediction in medium-cycle fatigue regime of notched specimens, Theoretical and Applied Fracture Mechanics 84 (2016) 140–148. doi:10.1016/j.tafmec.2016.03.006.

[25] Z.Wen, H. Pei, H. Yang, Y.Wu, Z. Yue, A combined CP theory and TCD for predicting fatigue lifetime in single-crystal superalloy plates with film cooling holes, International Journal of Fatigue 111 (2018) 243–255. doi:10.1016/j.ijfatigue.2018.02.020.

[26] M. Benedetti, V. Fontanari, C. Santus, M. Bandini, Notch fatigue behaviour of shot peened high-strength aluminium alloys: Experiments and predictions using a critical distance method, International Journal of Fatigue 32 (10) (2010) 1600–1611. doi:10.1016/j.ijfatigue.2010.02.012.

[27] M. Benedetti, V. Fontanari, M. Allahkarami, J. C. Hanan, M. Bandini, On the combination of the critical distance theory with a multiaxial fatigue criterion for predicting the fatigue strength of notched and plain shot-peened parts, International Journal of Fatigue 93 (2016) 133–147. doi:10.1016/j.ijfatigue.2016.08.015.

[28] M. Benedetti, C. Santus, Mean stress and plasticity effect prediction on notch fatigue and crack growth threshold, combining the theory of critical distances and multiaxial fatigue criteria, Fatigue & Fracture of Engineering Materials & Structures 42 (6) (2019) 1228–1246. doi:10.1111/ffe.12910.

[29] D. Li, D. Hu, R. Wang, Q. Ma, H. Liu, A non-local approach for probabilistic assessment of LCF life based on optimized effective-damage-parameter, Engineering Fracture Mechanics 199 (2018) 188–200. doi:10.1016/j.engfracmech.2018.05.041.

[30] Y. Ai, S.-P. Zhu, D. Liao, J. A. F. O. Correia, A. M. P. De Jesus, B. Keshtegar, Probabilistic modelling of notch fatigue and size effect of components using highly stressed volume approach, International Journal of Fatigue 127 (2019) 110–119. doi:10.1016/j.ijfatigue.2019.06.002.

[31] J. F. Barbosa, J. A. F. O. Correia, R. C. S. Freire Júnior, S.-P. Zhu, A. M. P. De Jesus, Probabilistic S-N fields based on statistical distributions applied to metallic and composite materials: State of the art, Advances in Mechanical Engineering 11 (8) (2019) 1–22. doi:10.1177/1687814019870395.

[32] R. C. Rice. Fatigue data analysis. ASM Handbook 2000 Vol. 8 Mechanical Testing and Evaluation. Edited by H Kuhn and D Medlin. ASM International. doi: 10.31399/asm.hb.v08.9781627081764.

[33] M. Lemaire, Structural Reliability, ISTE Ltd., 2009.

[34] R. C. Geary, The Frequency Distribution of the Quotient of Two Normal Variates, Journal of the Royal Statistical Society 93 (3) (1930) 442. doi:10.2307/2342070.

[35] J. H. Curtiss, On the Distribution of the Quotient of Two Chance Variables, The Annals of Mathematical Statistics 12 (4) (1941) 409–421. doi:10.1214/aoms/1177731679.

[36] G. Marsaglia, Ratios of Normal Variables and Ratios of Sums of Uniform Variables, Journal of the American Statistical Association 60 (309) (1965) 193–204. doi:10.1080/01621459.1965.10480783.

[37] D. V. Hinkley, On the ratio of two correlated normal random variables, Biometrika 56 (3) (1969) 635–639. doi:10.1093/biomet/56.3.635.

[38] G. Marsaglia, Ratios of Normal Variables, Journal of Statistical Software 16 (4) (2006) doi:10.18637/jss.v016.i04.

[39] A. Azzalini, A. Capitanio, The Skew-Normal and Related Families, Cambridge University Press, 2013.

[40] E. Díaz-Francés, F. J. Rubio, On the existence of a normal approximation to the distribution of the ratio of two independent normal random variables, Statistical Papers 54 (2) (2012) 309–323. doi:10.1007/s00362-012-0429-2.

[41] M. Benedetti, F. Berto, L. Le Bone, C. Santus, A novel Strain-Energy-Density based fatigue criterion accounting for mean stress and plasticity effects on the medium-to-high-cycle uniaxial fatigue strength of plain and notched components, International Journal of Fatigue 133 (2020) 105397. doi:10.1016/j.ijfatigue.2019.105397.

[42] ASM International, ASM Handbook, Volume 19: Fatigue and Fracture, ASM International, 1997.

[43] M. Benedetti, C. Santus, Notch fatigue and crack growth resistance of Ti-6Al-4V ELI additively manufactured via selective laser melting: A critical distance approach to defect sensitivity. International Journal of Fatigue 121 (2019) 281-292. doi:10.1016/j.ijfatigue.2018.12.020.

Tables

Table 1. Dependence of Williams power law singularity exponent and dimensionless N-SIF on the notch opening angle $\bar{\alpha}$, after Santus et al. [22].

$\bar{\alpha}$	s	$K_{N,UU}$
90°	0.4555	0.3210
60°	0.4878	0.2866

Table 2. p_i, q_i, c_i fit model coefficients for the limit values of l and λ, after Santus et al. [22].

Notch angle $\bar{\alpha} = 90°$, radius ratio range ρ = 0.01−1.0				
	p_1, q_1, c_1	p_2, q_2, c_2	p_3, q_3, c_3	p_4, q_4
l_{min}	1.5331595E−03	−5.4476787E−03	1.3930191E−02	4.3940341E−06
λ_{min}	4.3035219E−03	−2.0461370E−02	6.2189732E−02	−9.0345965E−06
l_{max}	−7.8790423E−02	1.8286498E−01	1.4527845E−01	-
Notch angle $\bar{\alpha} = 60°$, radius ratio range ρ = 0.01−1.0				
	p_1, q_1, c_1	p_2, q_2, c_2	p_3, q_3, c_3	p_4, q_4
l_{min}	3.4760317E−03	−1.0042167E−02	1.8482608E−02	1.3622097E−05
λ_{min}	1.2733490E−02	−3.9007230E−02	7.5860044E−02	1.0597477E−04
l_{max}	1.7783232E−02	8.5788750E−02	3.2189338E−01	-

Table 3. a_i fit model coefficients for the inversion of Eq. (10e).

a_1	a_2	a_3	a_4
2.6159	1.7983	-5.4302	4.1124

Table 4: Best-fit coefficients of the equations used to estimate NCV of l_{th} (Eq. (12a)) and l (Eq. (13a)).

Geometry	Notch angle $\bar{\alpha}$	NCV		Best-fit coefficients of Eq. (13d)			
		Symbol	value	n_1	n_2	n_3	n_4
Cracked	-	ν_{th}	2.842	-	-	-	-
Notched	90°	ν_0	3.125	0.1619	0.04948	0.998	0.957
	60°		2.910	0.1976	0.1141	0.987	0.345

Table 5: Best fit coefficients of the equations used to estimate mean value of l_{th} (Eq. (12b)) and l (Eq. (13d)).

Geometry	Notch angle $\bar{\alpha}$	NCV	Symbol	Index i	
				1	2
Cracked	-	ν_{th}	$m_{th,i}$	0.2640	0.08393
Notched	90°	ν_0	m_i	0.2486	0.06676
		4		0.2209	0.05860
		5		0.1971	0.05146
		6		0.1805	0.04720
		7		0.1675	0.04353
	60°	ν_0		0.2607	0.07603
		4		0.2269	0.06149
		5		0.2025	0.05619
		6		0.1829	0.05186
		7		0.1690	0.04774

Table 6: Best fit coefficients of the equations used to estimate skewness of l_{th} (Eq. (12c)) and l (Eq. (13e))

Geometry	Notch angle $\bar{\alpha}$	NCV	Symbol	Index i	
				1	2
Cracked	-	ν_{th}	$s_{th,i}$	0.06307	0.05287
Notched	90°	ν_0	s_i	0.05956	0.04688
		4		0.06288	0.04407
		5		0.06255	0.0444
		6		0.06264	0.04457
		7		0.06210	0.04481
	60°	ν_0		0.06393	0.05117
		4		0.06264	0.05162
		5		0.06347	0.05079
		6		0.06336	0.05103
		7		0.06300	0.05126

Table 7: Best fit coefficients of the equations used to estimate l_{lim} (Eq. (13b))

Notch angle $\bar{\alpha}$	NCV	b_1	b_2
90°	4	0.17590	0.1049
	5	0.08396	0.02717
	6	0.05615	0.01358
	7	0.04129	0.01157
60°	4	0.1651	0.05701
	5	0.08699	0.01692
	6	0.05960	0.007107
	7	0.04447	0.005942

Table 8. Requirements for statistically validated notch-derived l and threshold derived l_{th} estimations.

Requirements on l and l_{th}	Requirements on l
$\Sigma_{th}, \Sigma \le 0.07$ $0.5 \le \kappa_{th}, \kappa \le 2.2$	$l_{min} \le \bar{l} \le l_{max}$ $\nu = \nu(\bar{l}, \rho) \Rightarrow \nu \le 7$

Table 9: Best fit coefficients for the estimation of the normalized standard deviation on the estimation of notch fatigue limit (Eq. (14)).

Geometry	Notch angle $\bar{\alpha}$	NCV	Symbol	Index i					
				1	2	3	4	5	6
Cracked	90°	ν_{th}	$f_{th,i}$	1.263	1.826	0.1869	0.01150	0.947	1.85
	60°			1.264	1.639	0.1779	0.01195	0.979	1.87
Notched	90°	ν_0	f_i	1.262	1.561	0.1328	0.01360	0.985	1.76
		4		1.262	1.044	0.09107	0.007485	0.969	1.79
		5		1.257	0.7400	0.06425	0.003618	0.960	1.83
		6		1.257	0.5701	0.04643	0.002906	0.960	1.81
		7		1.253	0.4590	0.03567	0.002371	0.964	1.78
	60°	ν_0		1.264	1.567	0.1698	0.01146	0.989	1.85
		4		1.263	0.9417	0.08927	0.006158	0.998	1.85
		5		1.256	0.6725	0.05709	0.004405	1.01	1.80
		6		1.259	0.5196	0.04637	0.002588	0.984	1.85
		7		1.254	0.4196	0.03517	0.002010	0.992	1.83

Table 10: Best fit coefficients for the estimation of the normalized standard deviation on the estimation of crack threshold (Eq. (15)).

Geometry	NCV	Symbol	Value
Cracked	ν_{th}	d_{th}	1.90
Notched	ν_0	d	2.01 ($\bar{\alpha} = 90°$) 1.94 ($\bar{\alpha} = 60°$)
	4		2.38
	5		2.80
	6		3.26
	7		3.73

Table 11. High-cycle plain fatigue strength of investigated materials, after Santus et al. [23].

Material	Cycles to failure	Load ratio R	$\Delta\bar{\sigma}_{fl}/2$ (MPa)	$S/2$ (MPa)
7075-T6	3×10^7	-1	159	5.23
		0.1	116	9.4
42CrMo4+QT	1×10^7	-1	390	20.7
		0.1	337	5.3

Table 12. Statistical properties of threshold derived l_{th} estimations. Data in bold refer to estimations not compliant with the requirements set in Table 8.

Material	Load ratio R	$\Delta\bar{K}_{th}$ ($MPa\sqrt{m}$)	S_{th} ($MPa\sqrt{m}$)	$\bar{L}_{th}$ (mm)	Σ_{th} κ_{th}	$\mu_{th}/\bar{l}_{th}$ Eq. (12b) MC	δ_{th}/μ_{th} Eq. (12a) MC	sk_{th} Eq. (12c) MC
7075-T6	-1	4.2	0.30	0.0555	0.0556 2.2	1.009 1.009	0.158 0.159	0.318 0.320
	0.1	2.5	0.18*	0.0370	**0.0768** 0.89	1.026 1.026	0.224 0.222	0.756 0.743
42CrMo4 +QT	-1	9.1	0.66	0.0433	0.0636 1.4	1.015 1.015	0.183 0.182	0.480 0.471
	0.1	7.2	0.52	0.0363	0.0523 **0.22**	1.004 1.006	0.149 0.148	0.182 0.247

* Estimated from the scatter band reported in [42] based on six tests undertaken on three different material lots. The remaining experimental variants are assumed to have the same r_{th} ratio.

Table 13. Statistical properties of notch-derived *l* estimations. Data in bold refer to estimations not compliant with requirements set in Table 8.

Material	R (mm)	R	$\Delta\bar{\sigma}_{N,fl}/2$ (MPa)	$S_N/2$ (MPa)	$\bar{L}$ (mm) $\bar{l}$	Σ κ	ν	$\mu/\bar{l}$ Eq. (13e) MC	δ/μ Eq. (13a) MC	sk Eq. (13f) MC
7075-T6	0.12	-1	38.2	2.19	0.0520 0.00520	0.0467 1.7	4.4	1.012 1.013	0.204 0.201	0.341 0.333
		0.1	24.9	1.46	0.0362 0.00362	0.0707 0.72	4.9	1.045 1.047	0.348 0.348	0.818 0.818
	0.21	-1	42.0	2.69	0.0556 0.00556	0.0509 1.9	5.2	1.015 1.015	0.265 0.261	0.348 0.356
		0.1	27.0	1.43	0.0327 0.00327	0.0685 0.65	6.6	1.058 1.061	0.453 0.448	0.818 0.821
42CrMo4 +QT	0.21	-1	87.5	2.93	0.0273 0.00273	0.0444 0.63	**7.3**	1.027 1.029	0.324 0.319	0.513 0.510
		0.1	80.5	2.65	0.0367 0.00367	0.0258 2.1	6.2	1.004 1.004	0.161 0.159	0.166 0.171

Table 14. Predictions of notch fatigue limit based on validated threshold-derived l_{th} estimations.

Material	R	Predicted Geometry	Exp.		Statistical prop. of l_{th}		MonteCarlo	
			$\Delta\bar{\sigma}_{N,fl}/2$ (MPa)	$S_N/2$ (MPa)	$\Delta\bar{\sigma}_{N,fl}/2$ (MPa)	$S_N/2$ (MPa)	$\Delta\bar{\sigma}_{N,fl}/2$ (MPa)	$S_N/2$ (MPa)
7075-T6	-1	R1	62.3	2.86	62.0	4.47	62.0	2.27
		R0.21	42.0	2.69	42.3	3.50	42.2	2.30
		R0.12	38.2	2.19	39.2	3.45	39.1	2.42
	0.1	R1	45.0	2.72	43.7	4.29	43.7	3.62
		R0.21	27.0	1.43	27.9	3.06	27.9	2.66
		R0.12	24.9	1.46	25.2	2.95	25.2	2.58
42CrMo4 +QT	-1	R1	163	12.1	149	12.2	149	8.22
		R0.21	87.5	2.93	97.3	8.97	97.1	6.75

Table 15. Predictions of notch fatigue limit and crack threshold based on validated notch-derived l estimations. Data in bold refer to estimations not compliant with requirements set in Table 8.

Material	Notch geometry to get L NCV	R	Predicted Geometry	Exp.		Statistical prop. of l_{lim}		MonteCarlo	
				$\Delta\bar{\sigma}_{N,fl}/2$ (MPa) $\Delta\bar{K}_{th}$ (MPa $\sqrt{m}$)	$S_N/2$ (MPa) S_{th} (MPa $\sqrt{m}$)	$\Delta\bar{\sigma}_{N,fl}/2$ (MPa) $\Delta\bar{K}_{th}$ (MPa $\sqrt{m}$)	$S_N/2$ (MPa) S_{th} (MPa $\sqrt{m}$)	$\Delta\bar{\sigma}_{N,fl}/2$ (MPa) $\Delta\bar{K}_{th}$ (MPa $\sqrt{m}$)	$S_N/2$ (MPa) S_{th} (MPa $\sqrt{m}$)
7075-T6	R0.12 $\nu = 4.4$	-1	R1	62.3	2.86	61.6	3.84	61.6	2.36
			R0.21	42.0	2.69	41.6	3.35	41.5	2.64
			M(T)	4.2	0.30*	4.09	0.48	4.07	0.43
	R0.12 $\nu = 4.9$	0.1	R1	45.0	2.72	43.7	4.07	43.7	3.72
			R0.21	27.0	1.43	27.9	3.36	27.8	3.16
			C(T)	2.5	0.18*	2.53	0.49	2.50	0.48
	R0.21 $\nu = 5.2$	-1	R1	62.3	2.86	61.9	4.33	61.9	2.62
			R0.12	38.2	2.19	39.0	4.28	38.9	3.65
			M(T)	4.2	0.30*	4.20	0.62	4.17	0.57
	R0.21 $\nu = 6.6$	0.1	R1	45.0	2.72	43.4	4.01	43.4	3.77
			R0.12	24.9	1.46	24.6	3.85	24.4	3.66
			C(T)	2.5	0.18*	2.42	0.59	2.35	0.57
42CrMo4 +QT	R0.21 $\nu =$ **7.3**	-1	R1	163	12.1	144	8.52	144	8.07
			M(T)	9.1	0.66*	7.32	1.26	7.22	1.24
	R0.21 $\nu = 6.2$	0.1	R1	119	3.71	127	4.40	127	2.47
			C(T)	7.2	0.52*	7.25	0.63	7.23	0.59
*See note in Table 12 on the standard deviation of crack growth threshold.									

Figures (low resolution, then submitted in vector format)

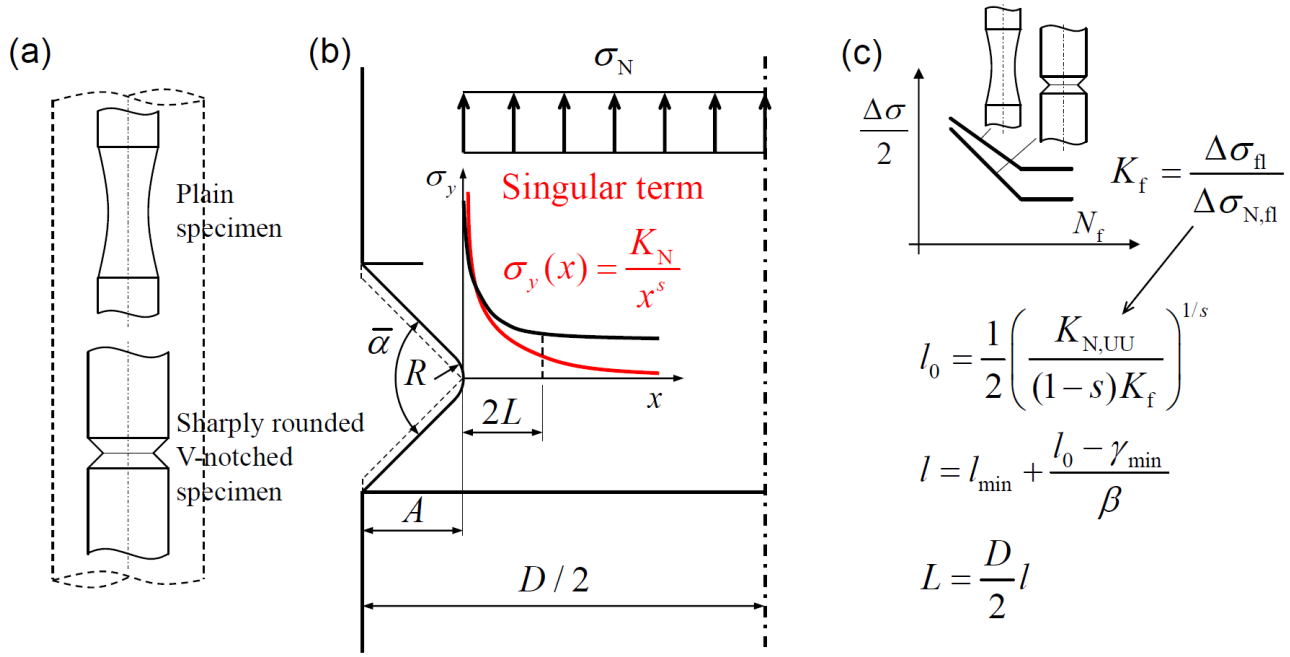

Figure 1. Specimen geometry for notch-derived estimation of the critical distance. (a) Specimen extraction from the same material bar, (b) characteristic dimensions and axial stress distributions, (c) summary of the critical distance inverse search.

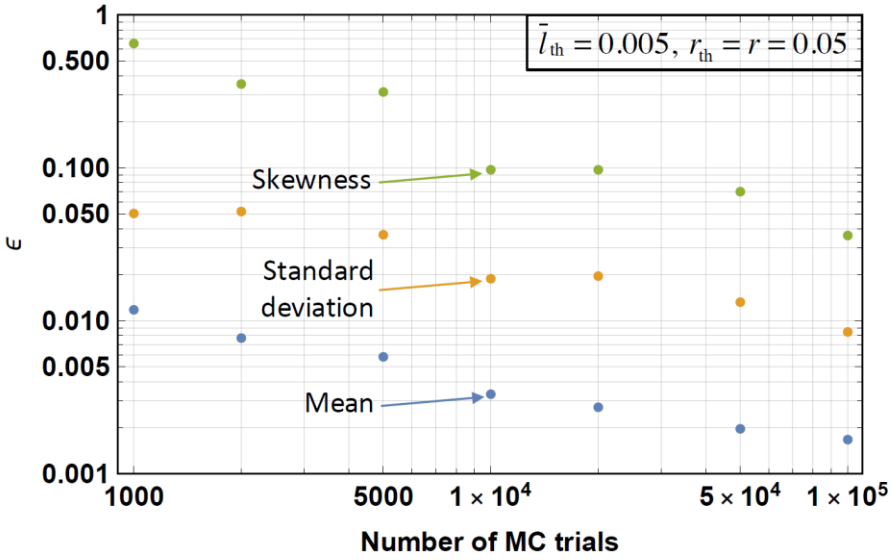

Figure 2. Convergence analysis aimed at determining the number of MC trials necessary to have stationary statistical properties. The fluctuation index ε is defined by Eq. (9).

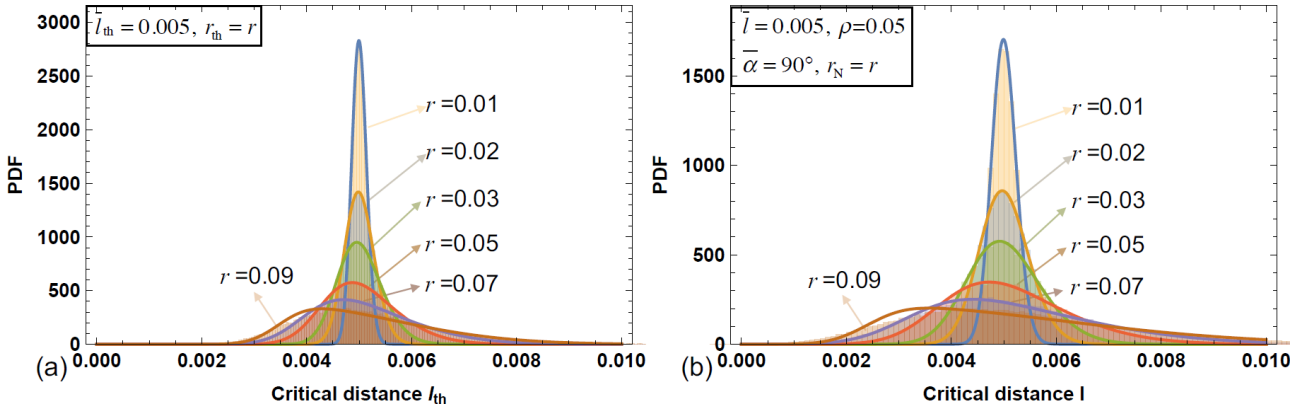

Figure 3. Probability density function of (a) threshold- and (b) notch-derived critical distance estimations. Histograms are obtained from MonteCarlo (MC) simulations. Mean, standard deviation and skewness calculated from MC simulations are used to evaluate the parameters of the skew-normal distributions plotted as solid lines. r is the coefficient of variation (CV) of the plain fatigue limit, which is here assumed to be equal to CV of crack threshold (r_{th}) and notch fatigue limit (r_N).

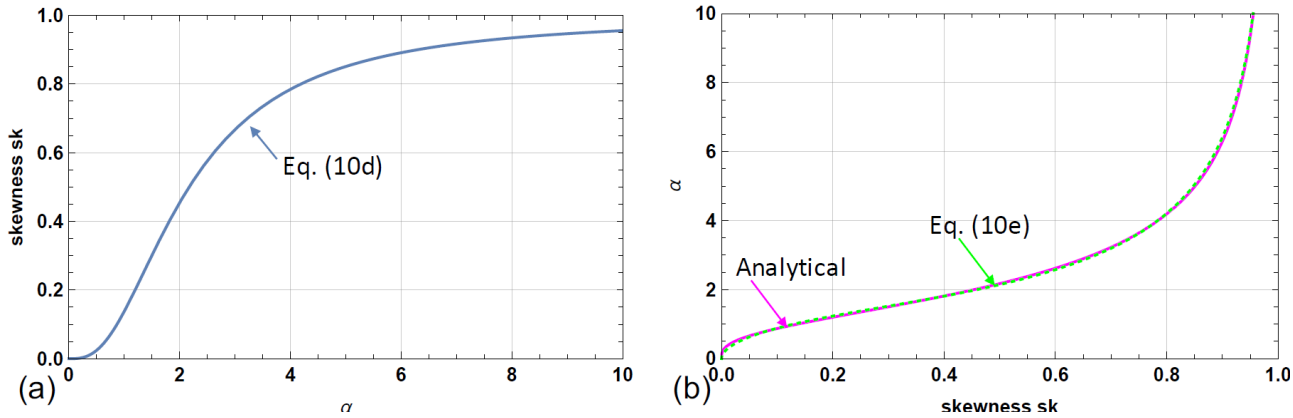

Figure 4. (a) relation between skewness and shape parameter α for the skew-normal distribution (Eq. (10d)). (b) comparison between analytical and numerical (Eq. (10e), dotted yellow line) inversion of Eq. (10d).

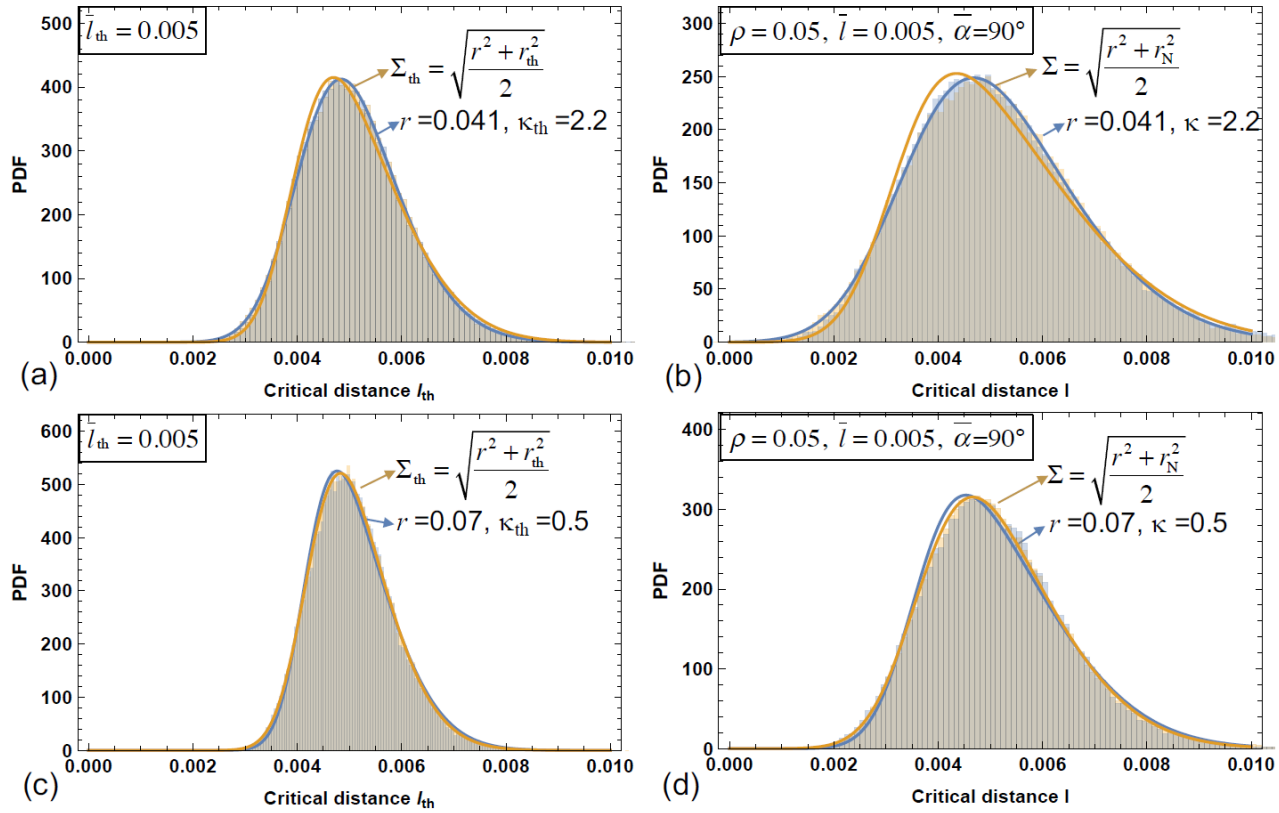

Figure 5. Probability density functions (PDF) of threshold- (a),(c) and notch-derived (b),(d) critical distance estimations. The PDFs accounting for the effective CV, r, $r_{th} = \kappa_{th}\, r$, $r_N = \kappa\, r$, are compared with those obtained considering, for plain fatigue limit, notch fatigue limit and the crack threshold, the same equivalent CV, namely Σ and Σ_{th}. (a) and (b) are obtained for the maximum, (c) and (d) the minimum value of the validity range established for κ and κ_{th}.

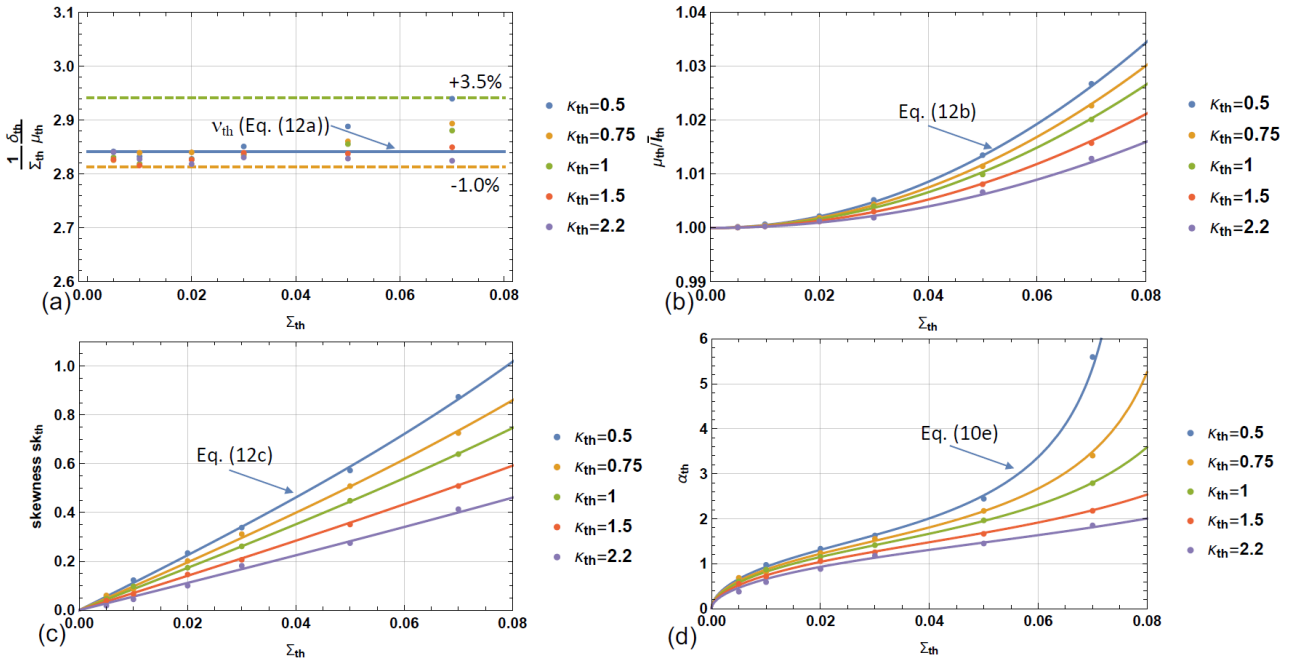

Figure 6. Statistical properties of l_{th}. (a) the CV normalized to Σ_{th} can be reasonably assumed to be a constant ν_{th}, thus independent of Σ_{th} and κ_{th} within an error band -1%, 3.5%. (b) The mean normalized to the input length $\bar{l}_{th}$ (estimated from mean of plain fatigue limit and crack threshold) is well represented by a hyperbolic function of Σ_{th} and κ_{th} (Eq. (12b)). (c) The skewness is well represented by a hyperbolic function of Σ_{th} and κ_{th} (Eq. (12c)). (d) Eq. (10e) can be used to infer the shape factor α_{th} from the skewness.

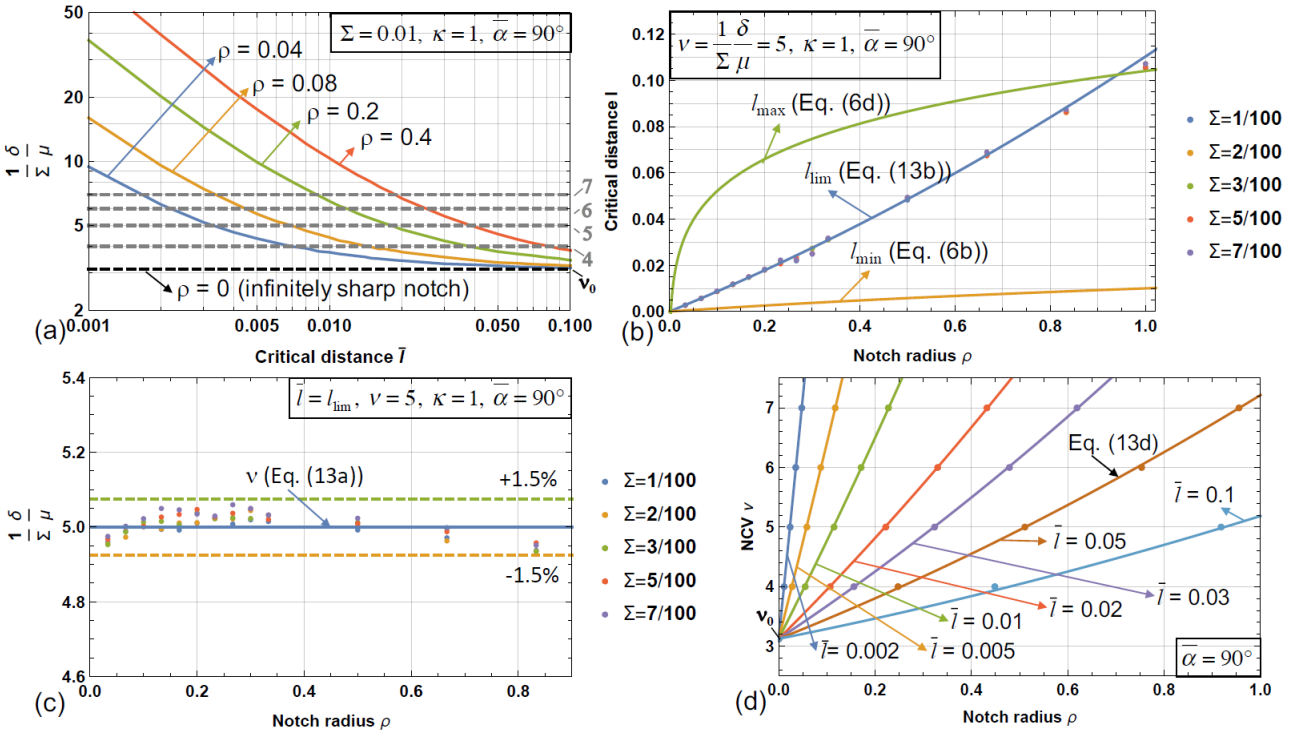

Figure 7. (a) The CV of notch-derived l estimations normalized to Σ (and denoted as ν) depends on the notch radius ρ. Here, the statistical properties of l will be evaluated considering five values of ν, ranging from ν_0 (corresponding to an infinitely sharp notch, black dashed line) to 7. (b) l_{lim} is the locus of critical distances for varying notch radii ρ corresponding to a certain value of ν (here taken equal to 5) and is compared with the extremes of the inversion validity range l_{min} and l_{max}. (c) The NCV ν for the locus l_{lim} is fairly independent of Σ and ρ within an error band -1.5%, 1.5%. (d) The dependency of ν upon ρ and $\bar{l}$ is well represented by Eq. (13d).

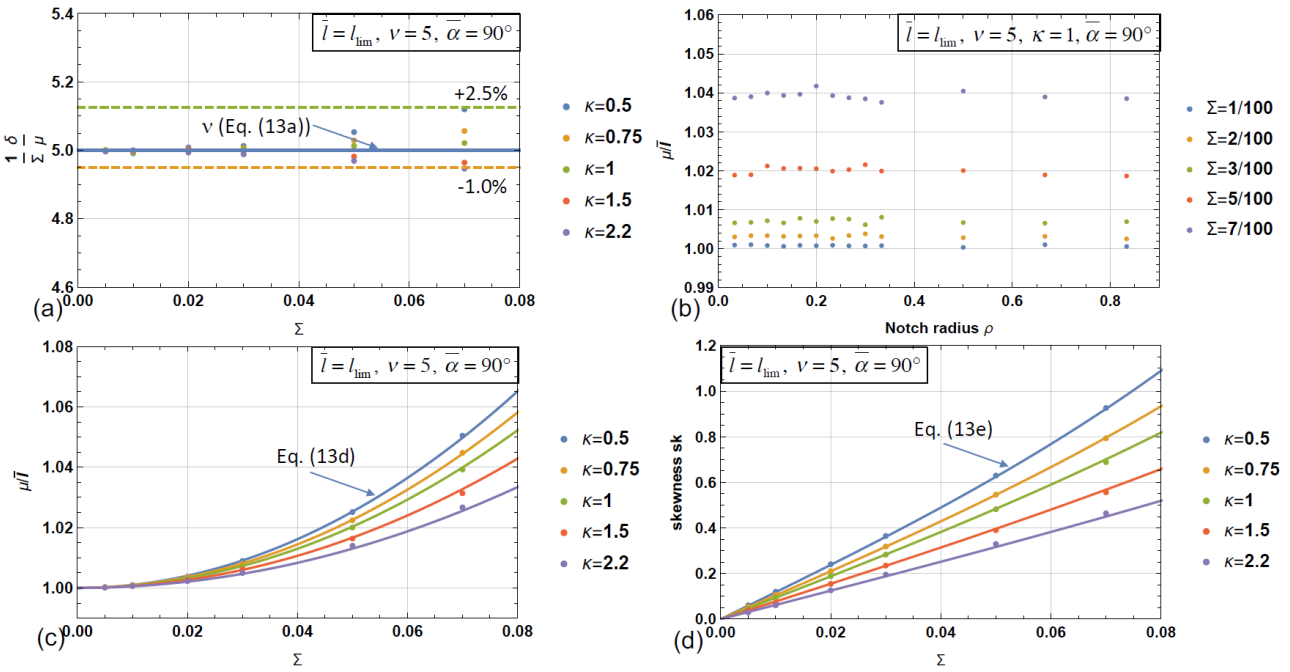

Figure 8. Statistical properties of notch-derived l estimations characterized by the same ν value (here taken equal to 5). (a) The NCV ν for the locus l_{lim} is fairly independent of Σ and κ within an error band -1.0%, 2.5%. (b) The mean normalized to the input length $\bar{l}$ (estimated from mean of plain and notch fatigue limit) is independent of the notch radius ρ. In the following, mean and skewness will be calculated as the average value obtained for the explored ρ values. The mean normalized to the input length $\bar{l}$ (c) and the skewness are well represented of hyperbolic functions of Σ and κ.

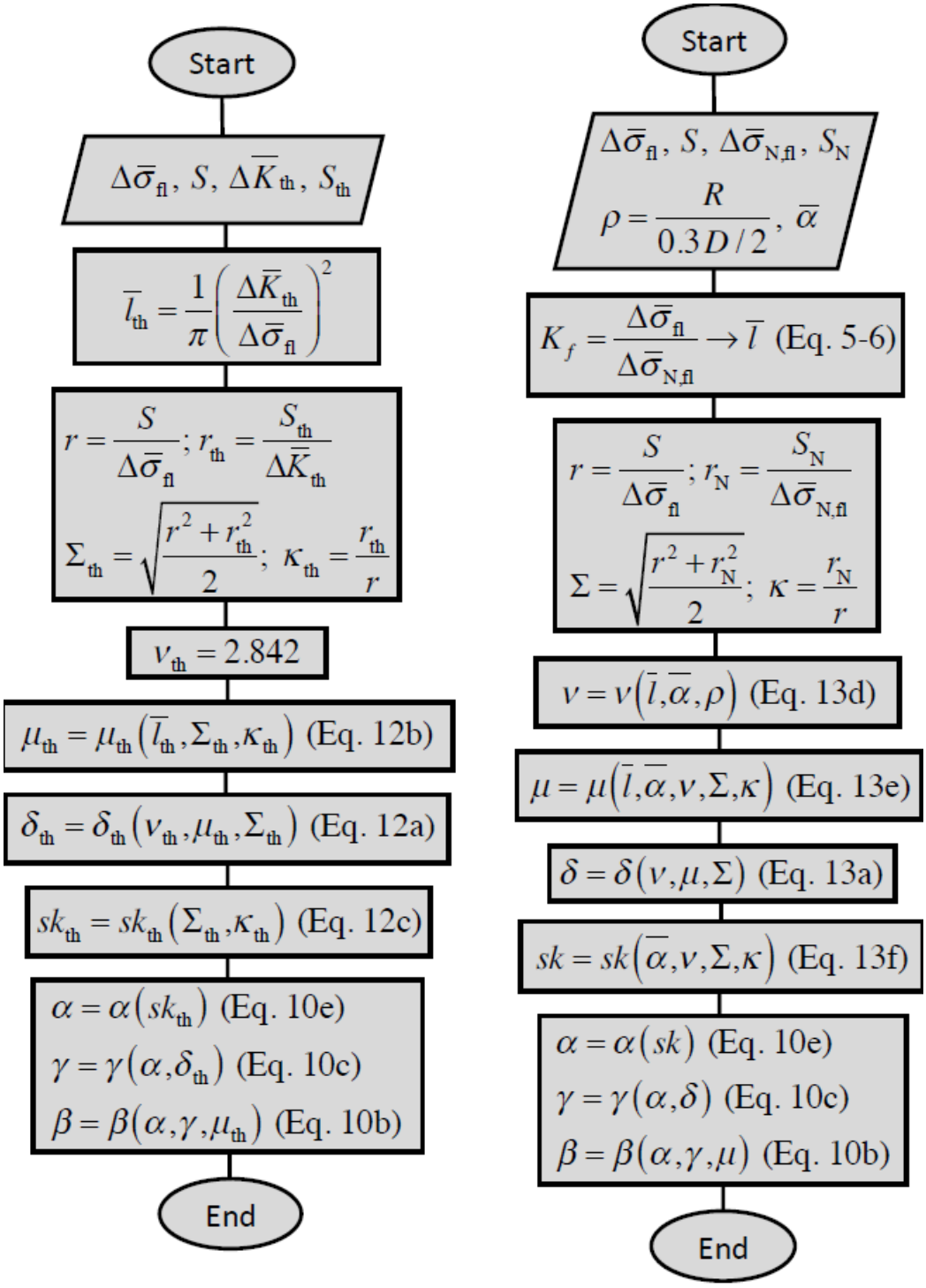

Figure 9. Flow-chart illustrating the step-by-step calculation procedure of the statistical properties of threshold- (left) l_{th} and notch-derived (right) l estimations.

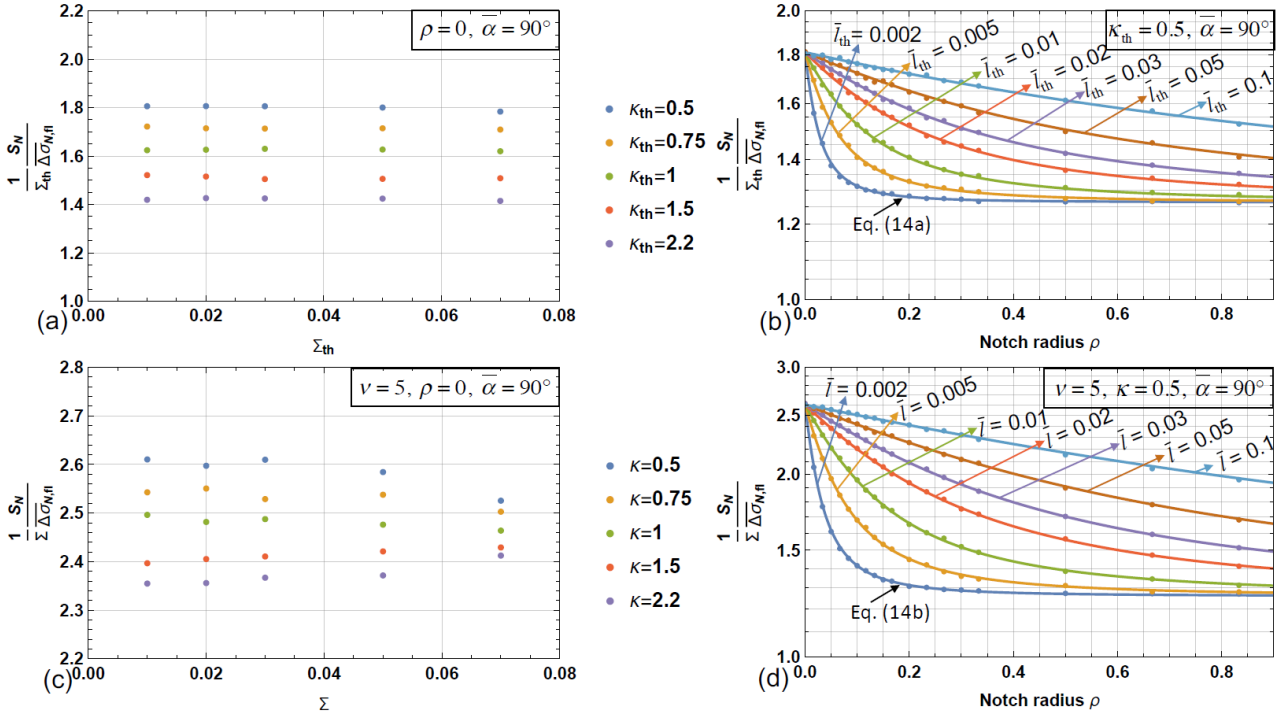

Figure 10. CV of notch fatigue strength estimations made using threshold- (a)-(b) and notch-derived (c)-(d) critical distance estimations and normalized to Σ_{th} or Σ. (a) and (c) refer to infinitely sharp notches and show that the largest value of NCV is obtained for κ_{th} or κ equal to 0.5. (b) and (d) show the dependency of NCV of notch predictions upon notch radius and input critical length.

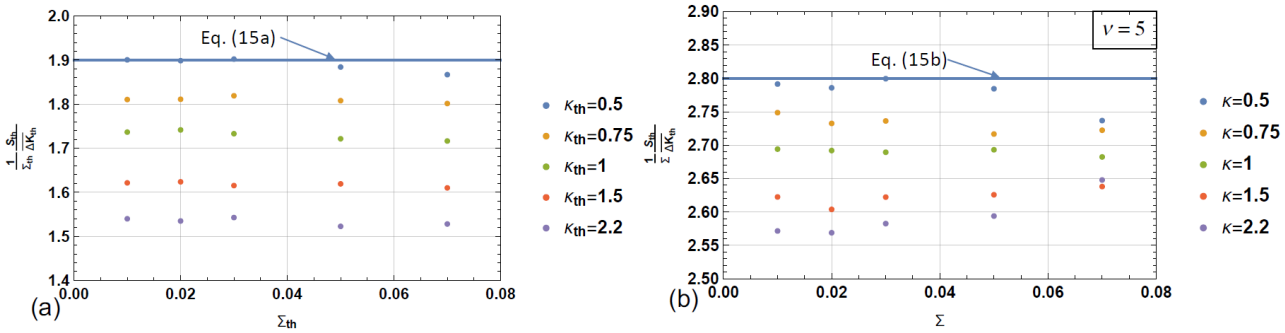

Figure 11. CV of notch crack threshold estimations made using threshold- (a) and notch-derived (b) critical distance estimations and normalized to Σ_{th} or Σ. They show that the largest value of NCV is obtained for κ_{th} or κ equal to 0.5 and will be used in the following as worst-case estimations.

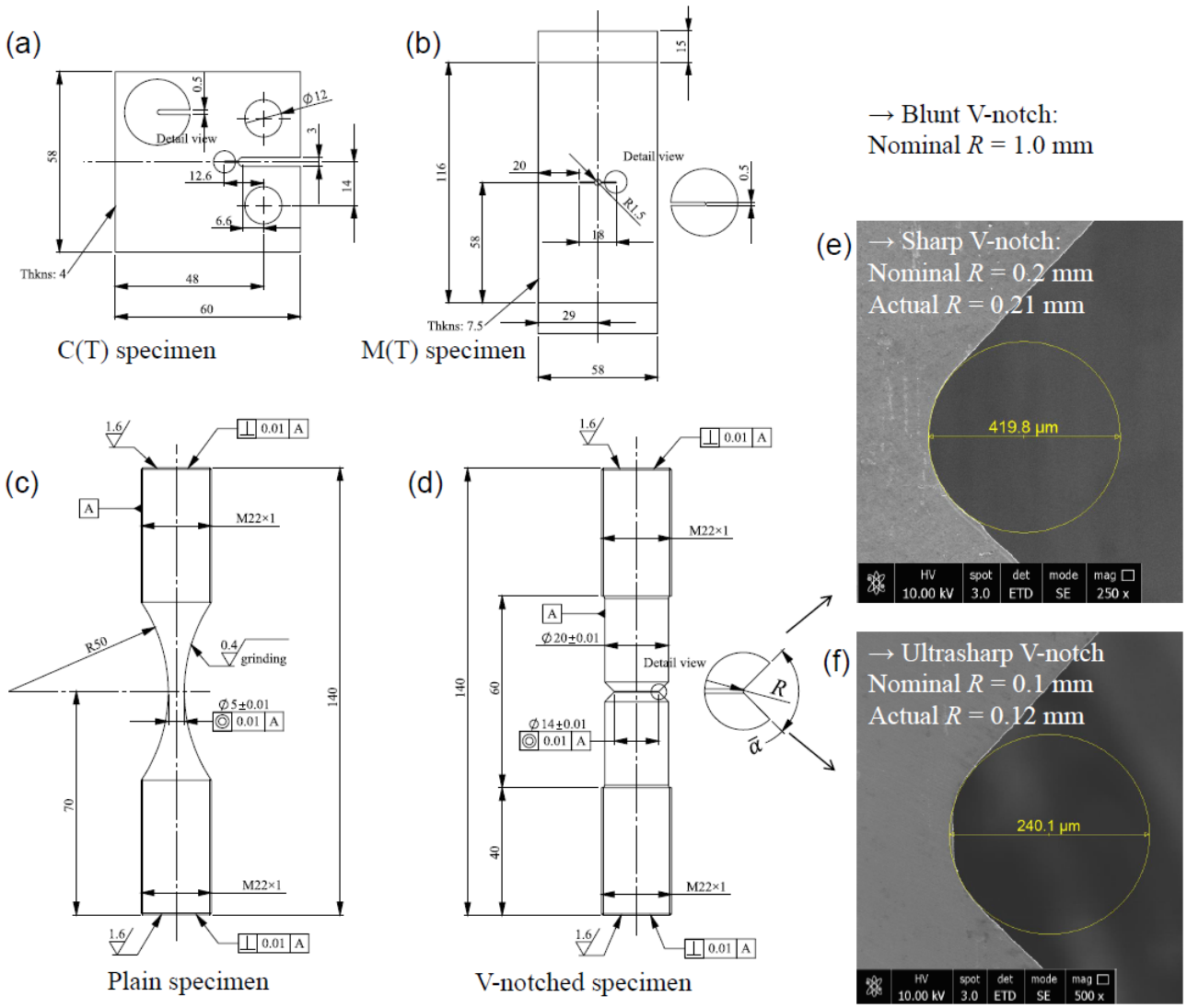

Figure 12. Technical drawing of the specimens used for the material data: (a) C(T) specimen, (b) M(T) specimen, (c) hourglass-shaped plain specimen, (d) V-notched specimen with $\bar{\alpha} = 90°$ and a generic notch radius. (e) Sharp notch with nominal radius R = 0.2 mm, and SEM evidence of the actual radius. (f) Ultrasharp notch with nominal radius R = 0.1 mm, and SEM evidence of the actual radius.

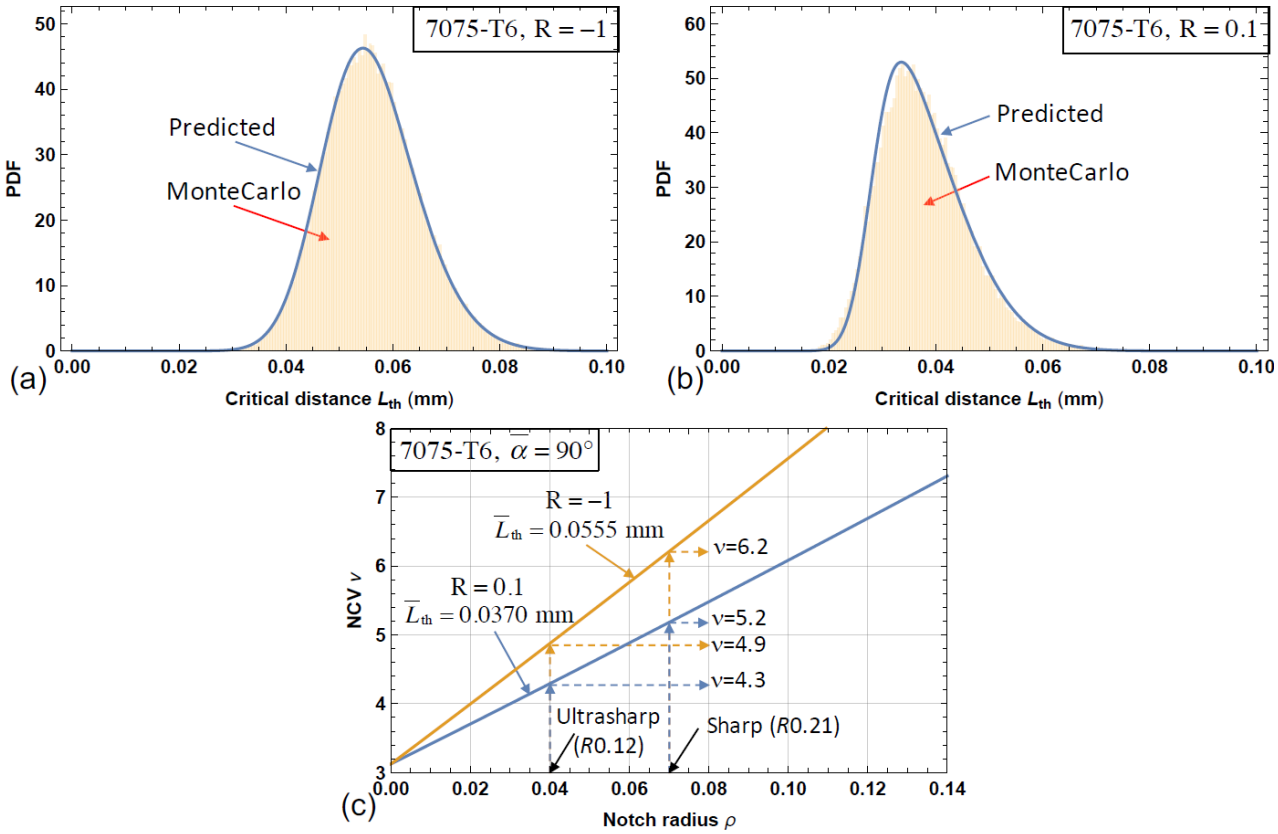

Figure 13. Comparison between PDF estimated through MC simulations and predicted by Eqs. (12) for the threshold-derived critical distance of 7075-T6 tested under (a) fully reversed and (b) pulsating axial fatigue tests. (c) The threshold-derived critical distance is input into Eq. (13d) to infer the NCV on the notch-derived critical distance estimations using notches of different sharpness.

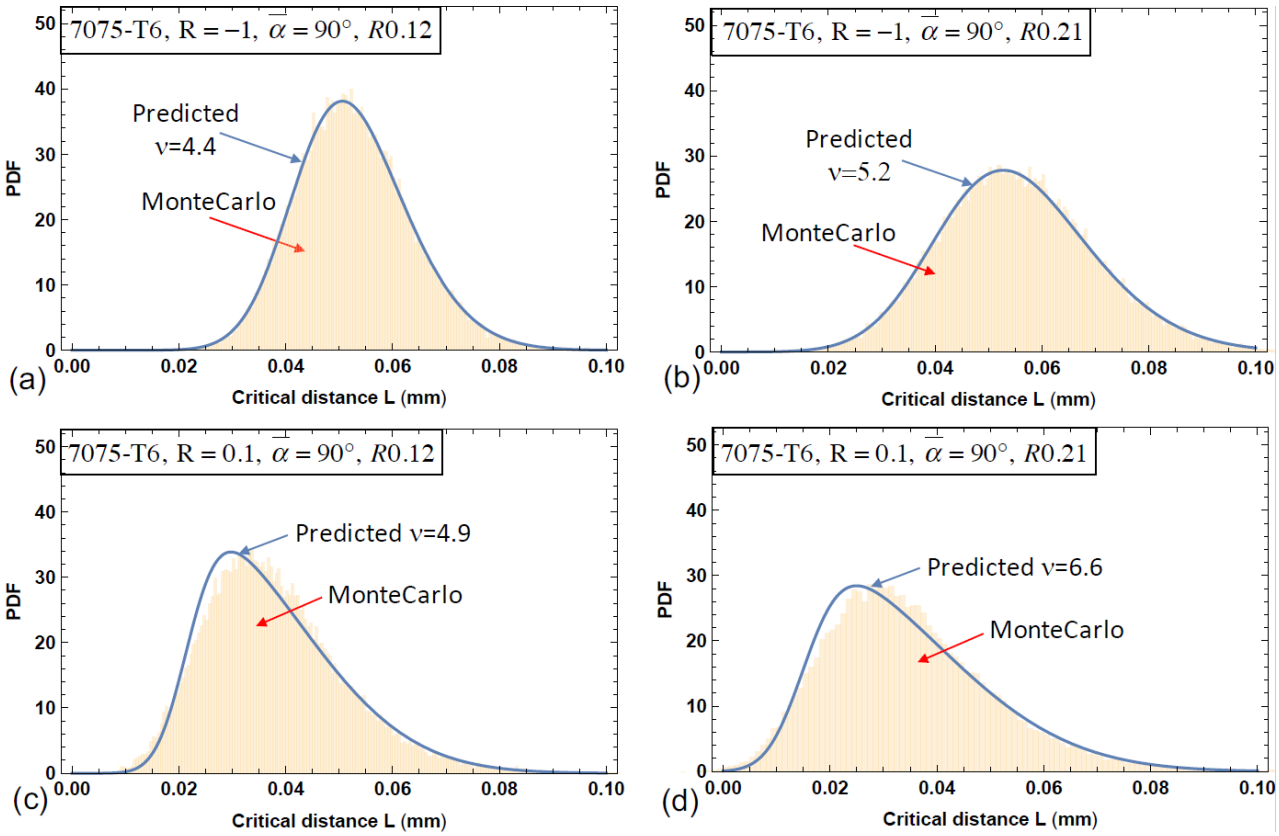

Figure 14. Comparison between PDF estimated through MC simulations and predicted by Eqs. (13) for the notch-derived critical distance of 7075-T6 tested under (a)-(b) fully reversed and (c)-(d) pulsating axial fatigue tests. (a)-(c) ultrasharp notches (*R*0.12), (b)-(d) sharp notches (*R*0.21).